Article

Cell

The Serotonergic System Tracks the Outcomes of Actions to Mediate Short-Term Motor Learning

Graphical Abstract

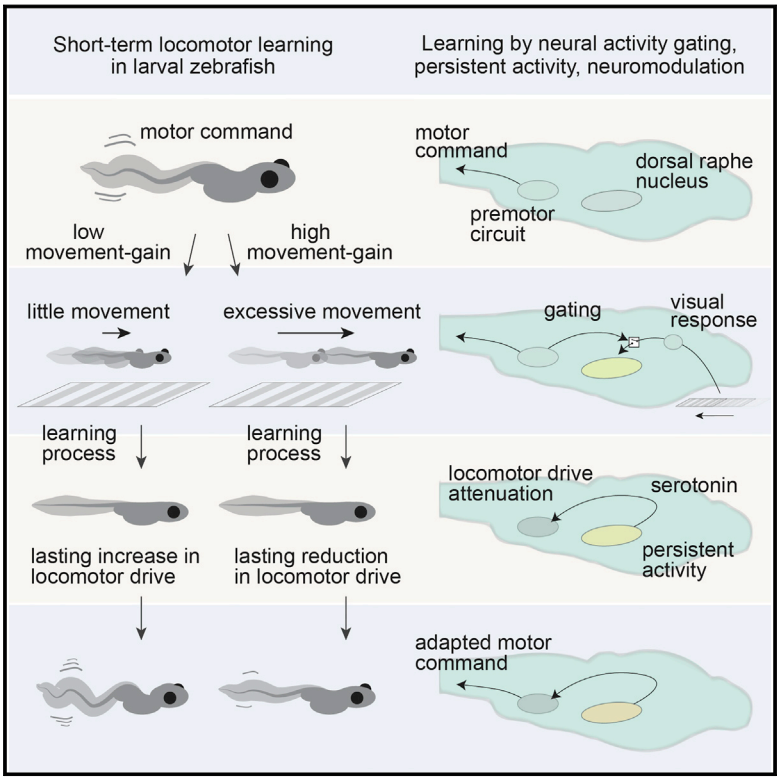

Highlights

- The dorsal raphe nucleus (DRN) mediates short-term locomotor learning
- DRN responses convey the visual outcomes of swim motor commands
- Learning induces a motor memory signal in the DRN that modulates future swimming
- DRN ablation/activation abolishes/extends the effect of learning

Authors

Takashi Kawashima, Maarten F. Zwart, Chao-Tsung Yang, Brett D. Mensh, Misha B. Ahrens

Correspondence

ahrensm@janelia.hhmi.org

In Brief

Animals use environmental feedback to learn the effectiveness of their movements: in larval zebrafish, this motor learning process is mediated by sensorimotor responses and persistent activity in serotonergic neurons in the dorsal raphe nucleus.

Kawashima et al., 2016, Cell *167*, 933–946
November 3, 2016
http://dx.doi.org/10.1016/j.cell.2016.09.055

CellPress

Article

Cell

The Serotonergic System Tracks the Outcomes of Actions to Mediate Short-Term Motor Learning

Takashi Kawashima,[1] Maarten F. Zwart,[1] Chao-Tsung Yang,[1] Brett D. Mensh,[1] and Misha B. Ahrens[1,2,*]
[1]Janelia Research Campus, Howard Hughes Medical Institute, 19700 Helix Drive, Ashburn, VA 20147, USA
[2]Lead Contact
*Correspondence: ahrensm@janelia.hhmi.org
http://dx.doi.org/10.1016/j.cell.2016.09.055

SUMMARY

To execute accurate movements, animals must continuously adapt their behavior to changes in their bodies and environments. Animals can learn changes in the relationship between their locomotor commands and the resulting distance moved, then adjust command strength to achieve a desired travel distance. It is largely unknown which circuits implement this form of motor learning, or how. Using whole-brain neuronal imaging and circuit manipulations in larval zebrafish, we discovered that the serotonergic dorsal raphe nucleus (DRN) mediates short-term locomotor learning. Serotonergic DRN neurons respond phasically to swim-induced visual motion, but little to motion that is not self-generated. During prolonged exposure to a given motosensory gain, persistent DRN activity emerges that stores the learned efficacy of motor commands and adapts future locomotor drive for tens of seconds. The DRN's ability to track the effectiveness of motor intent may constitute a computational building block for the broader functions of the serotonergic system.

INTRODUCTION

A range of behavioral modifications arises from motor learning, a process whereby sensory feedback is used to track the outcomes of actions, leading to adjustments of future motor commands to match outcome with intent. Multiple types of motor learning such as during limb coordination, reaching, and gaze stabilization are mediated by brain areas including the cerebellum, motor cortex, basal ganglia, and brainstem (Andalman and Fee, 2009; Boyden et al., 2004; Gao et al., 2012; Kawai et al., 2015; Morton and Bastian, 2006; Panigrahi et al., 2015; Raymond et al., 1996; Smith et al., 2006; Yin et al., 2009). Learning with what vigor to walk, swim, or fly to achieve a certain displacement is also essential for survival. The relationship between locomotor commands in the brain and the eventual displacement of the body in the environment is subject to frequent changes both in bodily properties such as muscle temperature or fatigue, and in environmental properties like water viscosity, terrain firmness, or wind. It is largely unknown which neural circuits underlie such forms of learning (Ahrens et al., 2012; Portugues and Engert, 2011) and by what mechanisms they mediate these processes.

Larval zebrafish swim in discrete bouts during which they must accurately traverse a desired distance. For example, when swimming against a water current to avoid being swept to potentially dangerous places, the distance traveled during a swim bout must be matched to the distance moved by the water current between bouts. However, the relationship between the strength of a neural swim command and the resulting distance swum, termed "motosensory gain," is subject to changing properties of an animal's body and environment. Larval zebrafish solve this tuning problem by adjusting "locomotor drive"—the number of action potentials at the neuromuscular junction during a swim bout—to compensate for changes in motosensory gain (Ahrens et al., 2012; Portugues and Engert, 2011). Further, as in all forms of motor learning, it is advantageous for animals to retain adapted locomotor drive for some time so that they do not have to re-adapt after every time they pause moving. Indeed, after sustained exposure to a given motosensory gain, larval zebrafish retain their adapted locomotor drive for extended periods of time (Ahrens et al., 2012).

Here, we identified, at the neural level, the operations and their loci underlying this form of short-term locomotor learning. Because it was unknown which brain areas were involved, we performed whole-brain neuronal activity imaging during fictive behavior in a virtual reality environment (Vladimirov et al., 2014). This screen implicated the dorsal raphe nucleus (DRN) of the central serotonergic system, an area previously associated with a variety of emotive, sensory, and motor functions (Dayan and Huys, 2015). We show that the DRN mediates short-term locomotor learning and present evidence that (1) DRN circuits detect self-generated movement consequences by motor-gated sensory coding in phasic neuronal activity, (2) the DRN stores information about movement consequences in persistent neuronal firing, and (3) it shapes future motor output by serotonergic modulation of downstream circuits.

RESULTS

Short-Term Locomotor Learning

To engage neural circuits participating in short-term motor learning, we placed paralyzed larval zebrafish in a virtual reality environment in which they fictively swim up a virtual stream in a one-dimensional track (Ahrens et al., 2012; Vladimirov et al., 2014) (Figures 1A and 1B). The stream is simulated by slow forward visual flow, which encourages swimming (Orger et al.,

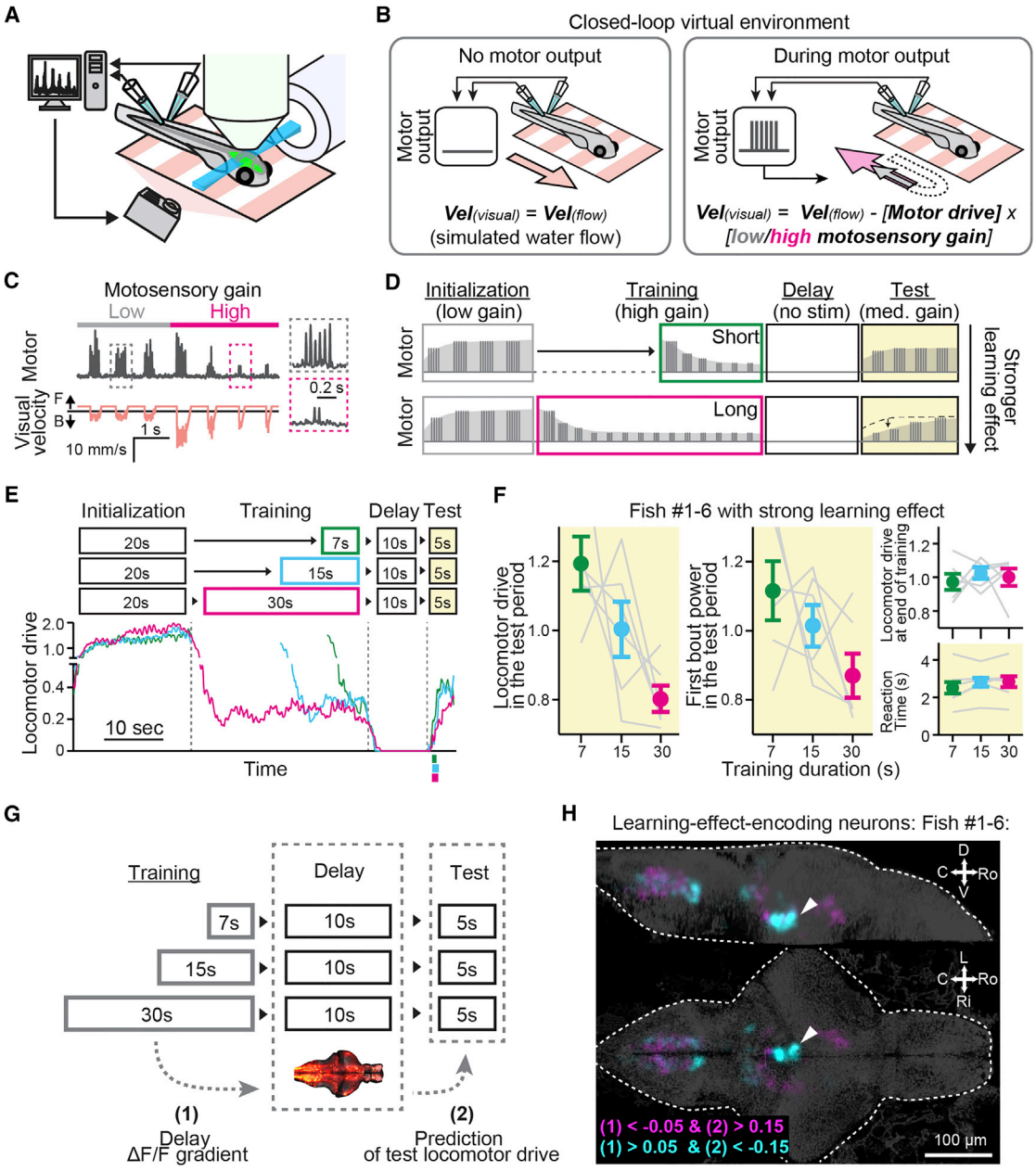

Figure 1. Whole-Brain Activity Mapping of Learning-Effect-Encoding Neurons

(A) Experimental setup. Signals from motor neuron axons (fictive swimming) trigger real-time visual feedback. A light-sheet microscope images the brain.

(B) Virtual environment. When the fish does not fictively swim (left), a visual scene moves forward slowly to elicit swimming. Fictive swim signals (right, inset) move the visual scene backward to mimic the effect of forward swimming. The speed of visual feedback is controlled by the motosensory gain. For the same swim bout, high gain yields more visual flow (magenta arrow) than low gain (gray arrow).

(C) Example swim trace and visual motion during a transition from low to high motosensory gain. "Motor" signal is the power in a sliding window of the tail voltage signal. Insets show zoom-ins of boxed regions.

(D) The short-term motor learning paradigm consists of repetitions of the initialization, training, delay, and test periods. No time passes during arrows between periods. Schematized electrophysiology traces represent the strength of fictive swim bouts. The learning effect is the dependence of locomotor drive in the test period on the duration of training.

(E) Representative fish behavior. Longer high-motosensory-gain training (magenta) more strongly attenuates locomotor drive in the test period. Colored lines below the x axis of the test period, mean ± SD of reaction times.

(F) Behavior across six fish with strong learning effect. Left: locomotor drive in the test period (average integrated swim power in the test period normalized by the average across three training conditions) is more attenuated after longer training. Right: locomotor drive at the end of training (top, last 5 s, normalized across

(legend continued on next page)

2008), as though the animal is trying to stay stationary relative to the visual surroundings. We record swim bouts electrically as activity in motor neuron axons in the tail (Ahrens et al., 2012; Masino and Fetcho, 2005). When a "fictive swim bout" is detected, we simulate the visual effect of forward swimming by thrusting the visual environment backward (Figure 1B). The velocity of this "movement" is proportional to the locomotor drive (that we measure from the tail as above) and is scaled by the visual motosensory gain (that we manipulate). Locomotor drive is an approximation of the number of spikes arriving at the neuromuscular junction of tail muscles during a swim bout. In nature, the motosensory gain (i.e., the amount of forward movement of the fish per unit of locomotor drive) varies due to muscle fatigue, muscle temperature, injury, changes in water viscosity, etc. These effects are simulated by manipulating the motosensory gain in virtual reality. Thus, [forward visual flow velocity] = [virtual stream velocity] – [locomotor drive] × [motosensory gain]. Fish rapidly adapt to changes in motosensory gain by adjusting locomotor drive to approximately equalize the travel distance induced by each swim bout (Figure 1C) (Ahrens et al., 2012; Portugues and Engert, 2011). This adjustment persists for tens of seconds, even after a "delay" period (detailed below) during which the fish does not swim. Thus fish retain a "motor memory" associated with the gain they were exposed to.

To probe mechanisms of motor learning, we developed a paradigm (Figure 1D) consisting of an initialization period in which 20 s of low motosensory gain is used to bring locomotor drive to a high baseline level, a training period of high motosensory gain to which the fish adjusts by attenuating locomotor drive, a delay period in which we apply 10 s of a constant visual stimulus that stops the animal from swimming, and a test period of 5 s to probe the extent to which the attenuated locomotor drive persists through the delay period. During the test period, an intermediate level of motosensory gain is applied.

Figure 1E illustrates the basic effect: that training-induced adaptation of locomotor drive persists beyond the delay period (all traces, test period) (Ahrens et al., 2012). This "motor memory" has several properties. The effect decays over tens of seconds (Figure S1A); we therefore refer to it as "short-term." Additionally, longer training periods (Figure 1E) result in stronger attenuation of locomotor drive both during the first swim bout of the test period (Figure 1F, center) as well as throughout the test period (Figure 1F, left). This property was robust enough to provide good statistical power for assessing the effects of subsequent experimental manipulations; thus we quantified the "learning effect" by the dependence of the test-period locomotor drive on the training duration.

Notably, locomotor drive was the same at the end of the different training durations (Figures 1E, 1F, and S1B). Thus, while real-time adaptation changed behavior quickly, the learning effect built up more slowly. The time to first swim bout in the test period was unaffected (Figures 1E, 1F, and S1C) suggesting that the training does not affect reactivity in general. Furthermore, the effect generalized to turning responses to sideways moving gratings and swim responses to a darkening stimulus (Burgess and Granato, 2007) in the test period (Figures S1D–S1I), where reaction time and response probability were similarly unaffected (Figures S1F and S1I), indicating an effect specific to motor vigor rather than general reactivity. Finally, the effect is not due to low levels of motor output inducing a prolonged state of torpor, because longer delay periods resulted in greater locomotor drive (Figure S1A).

Whole-Brain Activity Maps Reveal Persistent Signals in the Dorsal Raphe

To find loci mediating the persistent effects of learning, we performed whole-brain calcium imaging in larval zebrafish (Freeman et al., 2014; Vladimirov et al., 2014) in the motor learning paradigm (Figures 1A and 1E; Movie S1). The animals performed the task efficiently both with and without the scan laser present. The fish expressed the genetically encoded calcium indicator GCaMP6f (Chen et al., 2013) in almost all neurons, localized to cell nuclei (*Tg(elavl3:H2B-GCaMP6f)*^{jf7}). We automatically segmented the brain of each fish into 75,000–120,000 neurons (Figures S2A and S2B) and analyzed their activity (represented by fluorescence of the calcium indicator, ΔF/F). Simultaneous electrophysiological and optical recordings showed that the half decay time of the indicator was ~2 s (Figures S2C and S2D).

We applied a brainwide analysis to identify neurons that store a memory of the training as persistent neural activity during the delay period, a model based on previous studies of working memory (Machens et al., 2005; Major and Tank, 2004; Miri et al., 2011). Specifically, we postulated that the extent to which a neuron stores the learning effect is related to two properties of its delay-period activity: (1) the degree to which its average activity during the delay period is related in a graded manner to the duration of the training period (Figure 1G, (1)), as longer training leads to a stronger learning effect; and (2) the trial-by-trial correlation between the neural activity during the delay period and the locomotor drive in the subsequent test period (Figure 1G, (2)), as the learning should affect future behavior. We generated whole-brain functional maps of neurons whose parameters (1) and (2) exceeded threshold values in the subset of fish (6 out of 12) behaviorally exhibiting the strongest learning effect. We found a density of such "learning-effect-encoding neurons" in the dorsal raphe nucleus (DRN) (Figure 1H, arrowhead), a major serotonergic center in the vertebrate brain, located rostrally in the cluster of serotonergic nuclei in the zebrafish brainstem (Figure S3A) (Lillesaar et al., 2009; Parker et al., 2013; Yokogawa

conditions) and reaction time to the test stimulus (bottom) are similar across training durations. Gray lines, data from individual fish. Error bars, SEM across fish. Plots and statistics for all fish are in Figures S1B and S1C.

(G) Whole-brain analysis. Encoding of the learning effect was quantified by (1) dependence of a neuron's average ΔF/F activity signal in the delay period on the preceding training duration, and (2) degree to which a neuron's ΔF/F in the delay period predicts the locomotor drive in the subsequent test period (test locomotor drive) trial-by-trial.

(H) Functional brain map of neurons with parameters (1) and (2) exceeding thresholds, overlay from six fish with strong learning effect. A density of neurons occurs in the DRN (white arrow). Thresholds for extracting neurons are indicated at the bottom left (cyan for positive correlation to the learning effect; magenta for negative). See also Figures S2 and S3 and Movie S1.

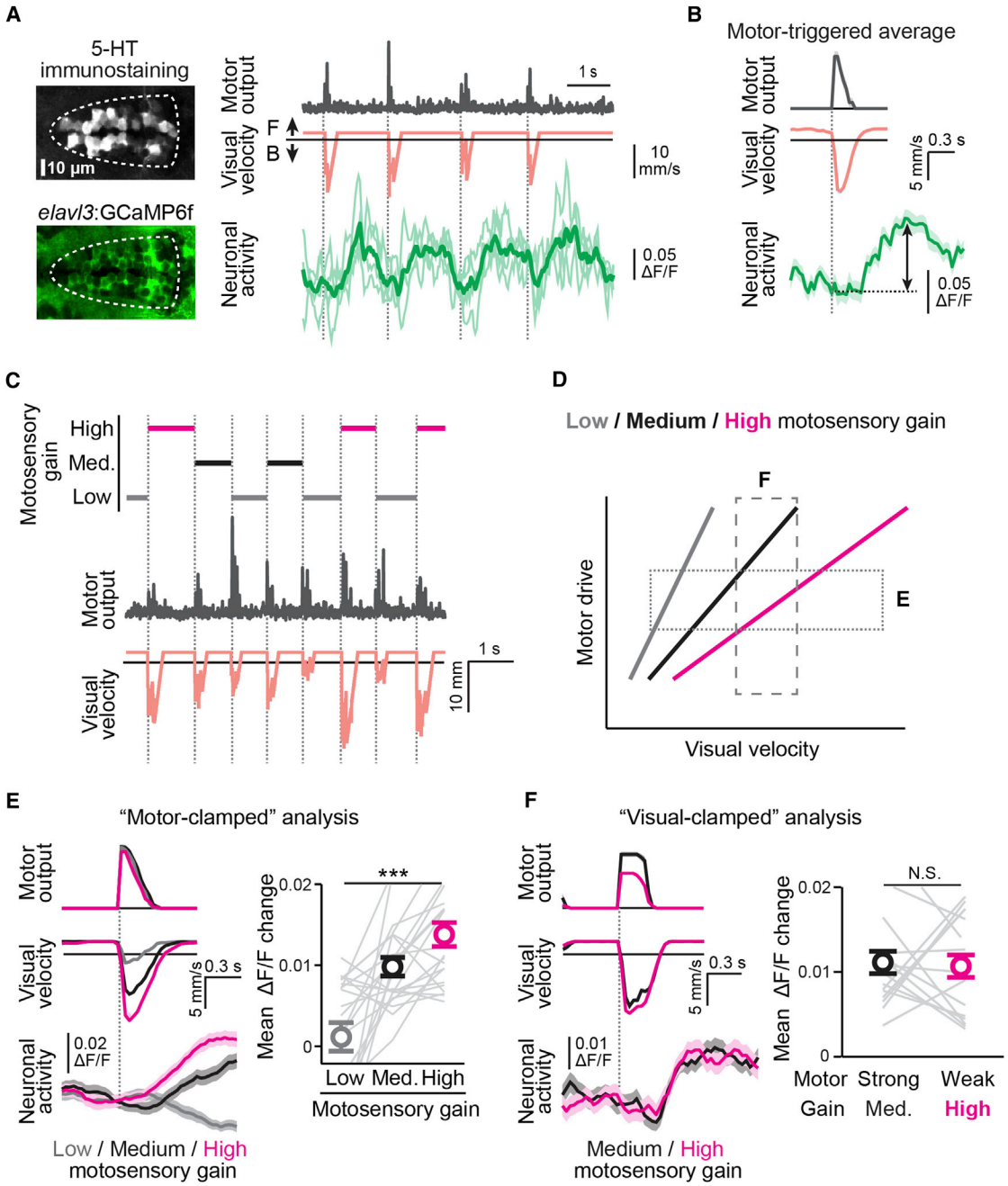

Figure 2. DRN Neurons Encode Sensory Feedback of Motor Action

(A) High-speed imaging of DRN neurons. Left: 5-HT immunostaining and GCaMP6f. Right: fictive swim signal, visual motion and ΔF/F activity of four group 1 DRN neurons (thick line is average ΔF/F).

(B) Example DRN neuron activity. Top: average locomotor drive across swim events aligned to bout onsets (dotted gray line). Middle: average visual velocity. Bottom: average ΔF/F of a group 1 DRN neuron. Black arrow: response magnitude used for analysis. Shadows, SEM across swim events.

(C) Stochastic gain paradigm. In a closed-loop environment, at every bout (gray, middle), motosensory gain is set randomly to low (dark gray), medium (black) or high (magenta).

(D) Analysis for (E) and (F). In motor-clamped analysis (E), visual coding is quantified by the dependence of the response on visual velocity within a restricted range of locomotor drive (data within horizontal bar). In visual-clamped analysis (F), motor coding is quantified by the dependence on locomotor drive within a restricted range of visual velocity (vertical bar).

(E) Motor-clamped analysis of DRN neurons' visual responses during the stochastic gain paradigm (see D). Left, average swim trace (top), visual motion (middle) and ΔF/F of a group 1 DRN neuron (bottom) under different motosensory gains. Right, dependence of group 1 DRN neurons' responses under different

(legend continued on next page)

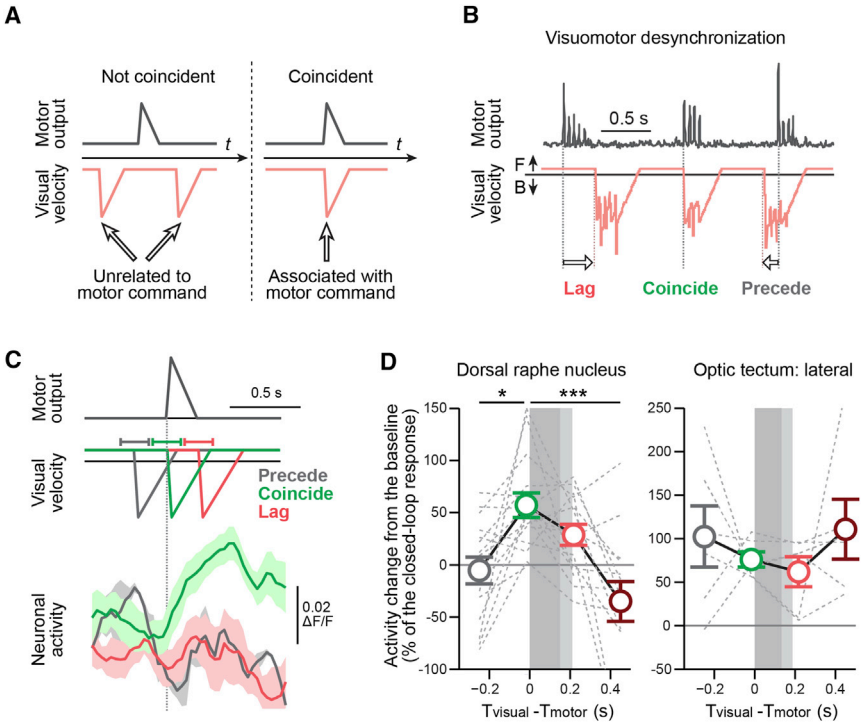

Figure 3. Motor Action Amplifies DRN Responses to Sensory Feedback

(A) Rationale for testing differences in DRN responses to visual motion during and without swimming.

(B) Temporal dissociation of visual motion and motor output by replaying in open-loop stimulus motion from a preceding closed-loop period (Figure S4F).

(C) Example group 1 DRN neuron response when visual motion precedes, coincides with or lags bout onset. Shadows, SEM across swim events. Bars over visual motion trace: binning windows for time gap between bout onsets and visual flow. Visual input activates this neuron when it occurs in a temporal window around bout onset time (green).

(D) Dependence of visual responses on timing of motor commands, averaged population data. Left: responses of group 1 DRN neurons when visual motion occurs with variable timing relative to bout onset. Responses were measured at a time relative to visual motion onset matching the time from motion onset to peak average response in closed-loop (800 ± 57 ms, 15 fish). Gray bars, average duration of bouts, aligned to the left edge. Light gray bars, SD of bout termination times. ΔF/F responses were averaged within equally sized bins centered on data points, normalized by the response during the closed-loop period described in Figure S4F in individual neurons, averaged within a fish, and further averaged across fish. $p = 4.6 \times 10^{-4}$ by one-way ANOVA, 15 fish. *p = 0.023; ***$p = 4.4 \times 10^{-4}$ by Tukey's post hoc test. Right: the same analysis for optic tectum neurons. Error bars, SEM, six fish. Gray dotted lines, data from individual fish.

et al., 2012). In fish with weak or no learning effect, there were few neurons whose parameters (1) and (2) exceeded threshold values (Figure S3B).

Subsets of DRN Neurons Encode Self-Generated Visual Feedback

To understand the signals driving DRN activity during training, we performed fast (30 Hz) light-sheet imaging of DRN neurons expressing GCaMP6f (Chen et al., 2013) in the cytosol (*Tg (elavl3:GCaMP6f)*^{jf1}) in fish swimming in a virtual environment (Figure 2A). To investigate neural coding during closed-loop behavior, we first extracted neurons that showed elevated activity in the presence of closed-loop feedback relative to open-loop forward-moving gratings (Figures S4A–S4C). These DRN neurons responded phasically (within ~800 ms) after each swim event (Figures 2B and S4D). Most of these (68% ± 6%, mean ± SEM across 21 fish) were monophasically activated after swim onset (Figure 2B, "group 1 neurons"). A smaller population of neurons (32% ± 6%) were initially suppressed and then gradually activated until the onset of the next swim bout (Figure S4D, "group 2 neurons").

Do these DRN neurons' phasic responses represent swim motor commands, visual motion, or a combination of visual and motor signals (Niell and Stryker, 2010; Seelig and Jayaraman, 2013)? We measured DRN responses in a "stochastic gain paradigm" where we randomly changed the motosensory gain at every swim bout, so we could independently assess the coding of motor and visual variables (Figure 2C). With randomized motosensory gain, the fish does not have time to substantially adapt, and average levels of locomotor drive across different gains are equalized. By selecting a small range of locomotor drive and inspecting how DRN neurons coded for the visual stimulus (Figure 2D, horizontal box), we found that average DRN phasic responses increased with the velocity of visual motion (Figures 2E and S4E). Conversely, by selecting a narrow range of visual velocities (Figure 2D, vertical box), we found that average DRN responses were invariant across levels of motor output (Figure 2F). These results show that, during swim bouts, subsets of DRN neurons phasically encode the speed of visual motion.

Critical to learning the relationship between motor output and sensory consequences is the ability to distinguish self-generated sensory feedback from externally generated sensory input. We asked whether DRN neurons respond to visual flow in general, or preferentially to visual flow that is temporally coupled to motor action (Figure 3A), using a closed-loop/open-loop paradigm.

motosensory gains. ***$p = 4.7 \times 10^{-9}$ for effect of motosensory gain by linear mixed-effects model (LME), 21 fish. Error bars, SEM across fish. Gray lines, data from individual fish.

(F) Visual-clamped analysis of motor-related responses of group 1 DRN neurons (see D). Left, example neuron with similar responses to events with different swim power but similar visual motion. Right, responses of DRN neurons across fish. Average response strength of group 1 neurons does not depend on locomotor drive. Error bars, SEM, 15 fish. Gray lines, data from individual fish.

See also Figure S4.

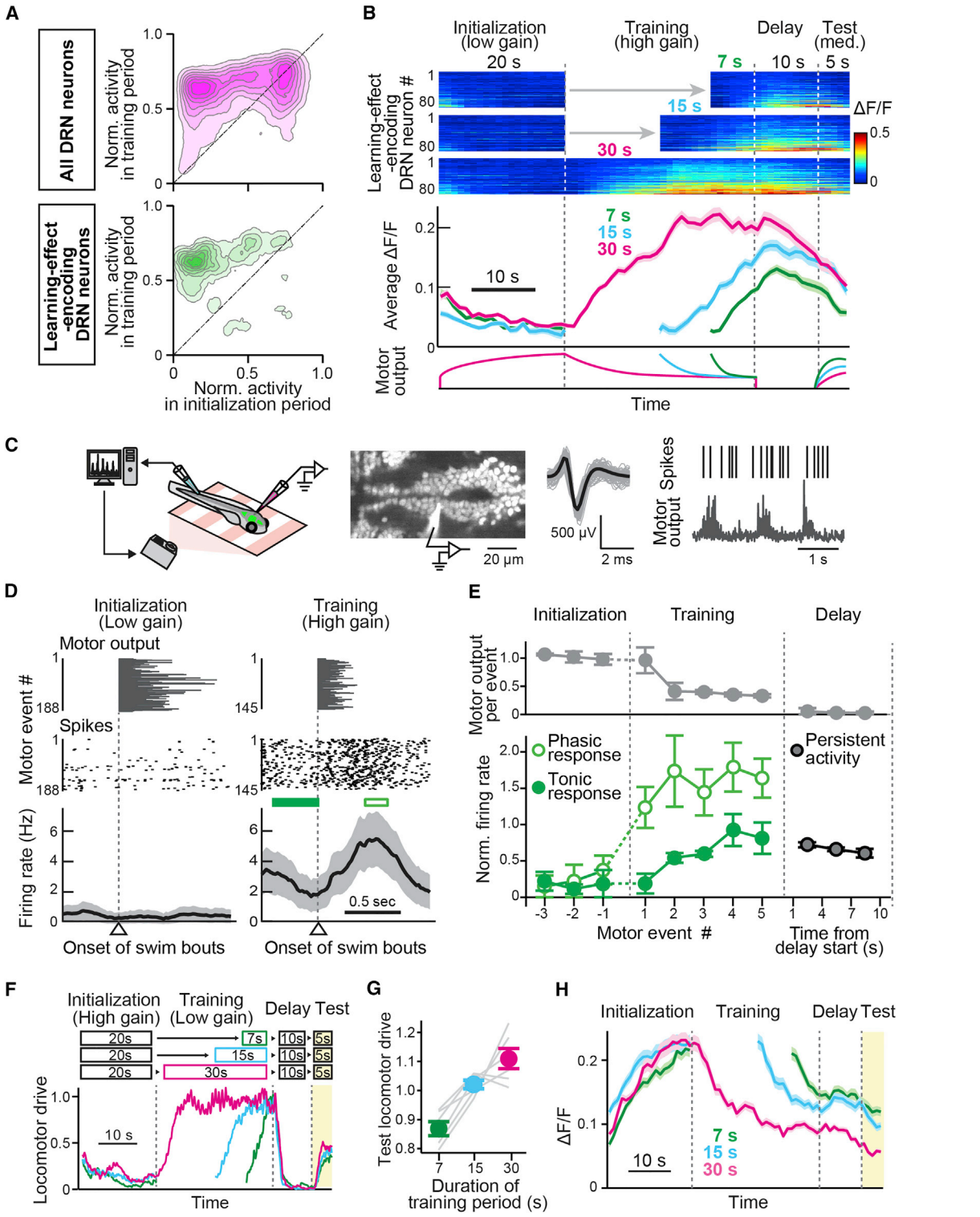

Figure 4. Activity of DRN Neurons during Short-Term Motor Learning

(A) Neural activity in the initialization and training periods of all DRN neurons in the motor learning paradigm. Top: density map of initialization versus training activity (4,254 DRN neurons in 12 fish). Bottom: density map of initialization versus training period activity of learning-effect-encoding DRN neurons (455 neurons from 12 fish, extracted as in Figure 1H).

(legend continued on next page)

First, the fish swam for 20 s in closed-loop under a fixed motosensory gain. Next, the same 20-s sequence of visual motion was replayed in open-loop (i.e., irrespective of fictive swimming, Figure S4F). Thus, during replay periods, swim bouts and visual flow were decoupled (Figure 3B), allowing us to determine whether DRN activation depended on their relative timing (Figure 3C). When visual flow occurred right after swim onset, DRN responses were stronger than when visual input and motor output were sufficiently desynchronized (example neuron in Figure 3C; average in Figure 3D). By contrast, in an area of the optic tectum that is also active during closed-loop swimming (Figure S4C), average visual responses were not significantly modulated by the co-occurrence of swim bouts (Figure 3D). Thus, a subset of DRN neurons preferentially responds to visual input that is self-generated and responds little to stimuli that arise from external sources—a key operation required for motor learning.

DRN Dynamics Reflect the Buildup and Maintenance of the Learning Effect

We tracked the activity of DRN neurons throughout repetitions of the motor learning paradigm to look for signatures of the buildup and retention of the learning effect. DRN neurons encoding the learning effect exhibited calcium signals that increased slowly during training (Figures 4A and 4B). During the subsequent delay period, the calcium signals decayed slowly but persisted for over 10 s. Due to the slow signal buildup, calcium signals at the end of training were greater after longer training; due to slow signal decay, activity throughout the delay period also depended on training duration. By varying the duration of the delay period, we found that the rate of activity decay was similar to that of the behaviorally probed learning effect (Figures S5A and S5B). These observations are consistent with a model in which the learning effect is encoded in persistent activity of DRN neurons.

To obtain insight into the spiking dynamics of DRN neurons at the millisecond timescale and to test whether the dynamics observed with functional imaging are not an artifact of measuring calcium levels, we made electrophysiological cell-attached recordings from single DRN neurons in fish performing the short-term motor learning task (Figure 4C). We observed a fast (phasic) response that occurred after swim bout onset (Figure 4D), but only during high motosensory gain, consistent with calcium measurements of phasic responses (Figures 2 and 3). In addition, we found a slow (tonic) component—the spike rate measured right before a swim bout—that evolved over multiple seconds and also only appeared during high motosensory gain (Figure 4E). Whereas the phasic component appeared immediately after the start of the training period, the tonic component increased slowly over the course of multiple swim bouts after the transition (Figure 4E). Finally, tonic DRN neuron activity persisted during the delay period, decaying slightly over 10 s (Figure 4E). Consistent with the calcium imaging results, these observations provide support for a model in which the DRN integrates information about motor-command consequences—in the form of visual flow velocity—to build up its persistent activity.

Above we showed that high motosensory gain training leads to a persistent increase in DRN activity and reduction of locomotor drive. We tested the opposite effect by training under low motosensory gain for varying amounts of time (Figure 4F). Here, longer training resulted in more enhanced locomotor drive in the test period (Figures 4G and S5C) and activity of DRN neurons was inverted compared to the high motosensory gain training assay (Figure 1), with increased activity during the high-gain initialization period and gradually decreasing activity in the low motosensory gain training period. Thus, low motosensory gain training also results in motor learning and training-duration-dependent signals in the DRN (Figures 4H and S5D).

Cell-Type-Specific DRN Dynamics

We asked whether the various cell types of the DRN, which include serotonergic and GABAergic neurons (Weissbourd et al., 2014), exhibit different activity dynamics during short-term motor learning. We repeated the motor learning experiment (as in Figure 1) in fish expressing GCaMP6f localized to the nucleus in most neurons and a co-label in either serotonergic or GABAergic neurons (STAR Methods). Serotonergic neurons (Figures 5A and 5B) mostly exhibited activity patterns similar to those described above in learning-effect-encoding neurons (Figures 4A and 4B), with increased activity during the high motosensory gain period and slow decay during the delay period (Figure 5C). By contrast, GABAergic neurons (Figure 5D) exhibited more diverse activity dynamics (Figure 5E)—most (57% ± 5%) were activated during both the initialization and

(B) Dynamics of learning-effect-encoding DRN neurons during the motor learning paradigm. Top: trial-averaged ΔF/F from 80 individual DRN neurons in a representative fish selected by parameters (1) and (2) in Figure 1G and ordered by overall activity. Middle, ΔF/F traces averaged over these neurons. Shadows, SEM across neurons. Bottom: schematic of locomotor drive.

(C) Single-cell loose-patch DRN recordings. Left: spikes from a DRN neuron are recorded during fictive swimming. Middle: two-photon guided targeting of a DRN neuron and example spike waveform. Bottom: spike raster plot and fictive swims.

(D) Representative DRN neuron spiking under low (initialization) or high (training) motosensory gain. Individual fictive swim traces (top; length indicates bout duration) and spike times (middle) are aligned to bout onsets (dotted lines). Bottom: mean firing rate of the neuron. Shadows, 95% confidence intervals from the binominal distribution. Horizontal green boxes at the top: windows for calculation of tonic (dark green) and phasic (light green) firing rates in (E).

(E) Summary of DRN spiking dynamics across individual swim bouts before and after a change from low to high motosensory gain. Tonic firing rates (window just before bouts) and phasic firing rates (just after bouts) as indicated by horizontal green boxes in (D). Firing rates during the delay period are the mean firing rates in successive 3-s bins normalized by overall mean firing rate (2–4 Hz) during training in individual neurons and averaged across three DRN neurons. Error bars, SEM across neurons.

(F) Motor learning paradigm for assessing buildup of the learning effect during low-motosensory-gain training. Top: behavioral paradigm. Bottom: representative fish with increased locomotor drive during training and enhanced locomotor drive in the test period after longer training.

(G) Dependence of locomotor drive in the test period on training duration across six fish with strong learning effect. Gray lines, data from individual fish. Error bars, SEM across fish. Plots and statistics for all tested fish are in Figure S5C.

(H) Average calcium traces of 192 DRN neurons from a representative fish in the paradigm in (F). Activity traces of neurons with peak activity during initialization were extracted and averaged. Shadows, SEM across averaged neurons.

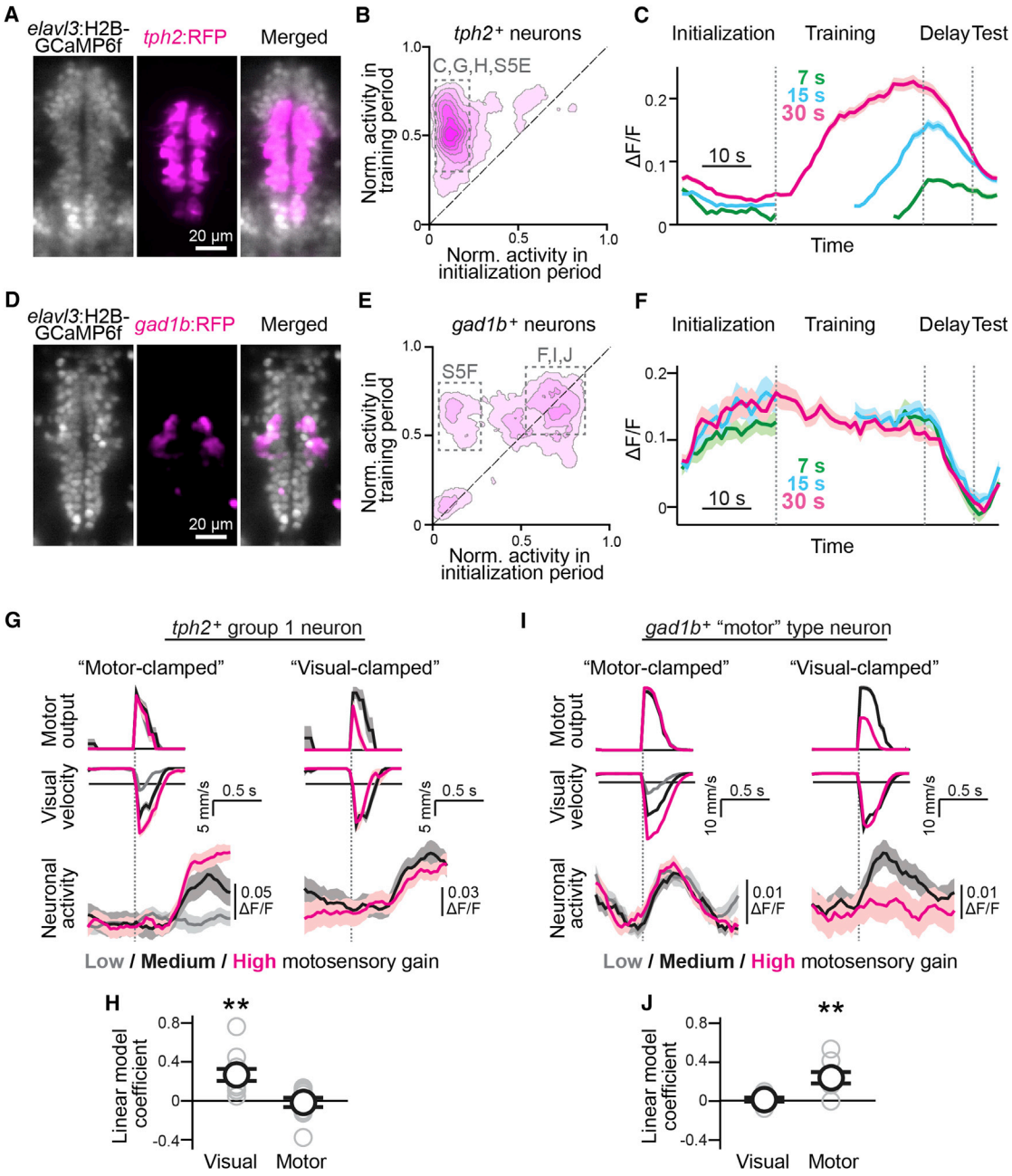

Figure 5. Cell-Type-Specific DRN Dynamics

(A–C) Dynamics of serotonergic DRN neurons during the motor learning paradigm. (A) Double labeling of DRN neurons with H2B-GCaMP6f (gray) and serotonergic DRN neurons with RFP (magenta). (B) Activity in the initialization and training periods of 420 serotonergic neurons across seven fish, same analysis as in Figure 4A. Activity is higher during training for most neurons. (C) Dynamics of serotonergic neurons during formation and retention of the learning effect of neurons in box C in (B), averaged over 11 trials and across 94 *tph2*$^+$ DRN neurons in one representative fish. Shadows, SEM across neurons.

(D–F) Dynamics of GABAergic DRN neurons during the motor learning paradigm. (D) Double labeling of DRN neurons with H2B-GCaMP6f (gray) and GABAergic neurons with RFP (magenta). (E) Activity in the initialization and training periods of 356 neurons from nine fish. (F) Dynamics of GABAergic neurons in box F in (E), averaged over 11 trials and across 47 *GAD1B*$^+$ neurons for one representative fish, showing activation when fish swims (initialization, training, test) and rapid decay when it does not (delay). Shadows, SEM across neurons.

(G–J) Neural activity imaged at 30 Hz during the stochastic gain paradigm of Figure 2C. Sources of population data are indicated by boxes in (B) and (E).

(G) Responses of an example group 1 serotonergic neuron represented by (left) dependence on visual stimulus velocity by motor-clamped analysis as in Figure 2E and (right) dependence on locomotor drive by visual-clamped analysis as in Figure 2F.

(legend continued on next page)

training periods (in which the fish swam) but not during the delay period (in which the fish did not swim) (Figures 5E and 5F). A small subpopulation of GABAergic neurons (18% ± 5%) showed activity patterns similar to the serotonergic neurons (Figure 5E).

To inspect cell-type-specific DRN activity with finer temporal resolution, we performed 30 Hz imaging in fish expressing GCaMP6f in the cytosol with a co-label in either serotonergic or GABAergic neurons. We imaged the same sets of neurons in the motor learning paradigm (Figure 1) and the stochastic gain paradigm (Figure 2), so that we could examine the relationship between fast and slow DRN dynamics (Figures 5B and 5E). Serotonergic neurons that were activated during the training period of the motor learning paradigm (Figure 5B) fell into two categories resembling the "group 1" (73% ± 8%) and "group 2" (27% ± 8%) neurons described in Figures 2 and S4D. On average, group 1 neuronal responses occurred after the onsets of swim bouts, with response amplitude depending on the speed of visual feedback, but not on the power of individual swim bouts (Figures 5G and 5H). Average activity of group 2 serotonergic neurons rose at a later time after swim bouts, and response amplitude also depended on the speed of visual motion (Figure S5E).

GABAergic neurons' fast dynamics differed depending on their activity profiles during the motor learning task (Figure 5E). The average response of GABAergic neurons that showed elevated activity in both the initialization period and training period depended on the power of individual swim events, but not on the speed of visual feedback (Figures 5I and 5J). GABAergic neurons that showed elevated activity in the training period showed activity dynamics similar to the group 2 serotonergic neurons, with a delayed response to visual feedback from the previous swim bout (Figure S5F). These results show that distinct cell types in the DRN encode different behavioral and sensory quantities.

The DRN Causally Underlies the Learning Effect

We tested whether manipulating DRN activity perturbs learning. First, we blocked serotonin release and synthesis in axon terminals by bath application of para-chlorophenylalanine (pCPA) (Borue et al., 2009). Compared to untreated fish, pCPA-treated fish showed significant impairment in learning (Figures 6A and 6B). We next tested whether ablation of serotonergic neurons affects the learning by using a transgenic zebrafish, *Tg(tph2:epNTR-RFP)*^{if41}, expressing the nitroreductase epNTR, which converts the prodrug metronidazole (MTZ) into a cytotoxic product (Tabor et al., 2014), directly under the *tph2* promoter (Yokogawa et al., 2012) (Figure 6C). This ablation also led to a significant impairment in learning (Figure 6D). Neither pCPA treatment nor nitroreductase-mediated ablation caused general impairment in the ability to swim, in the optomotor response, or in real-time motor adaptation (Figure S6). These results indicate that the serotonergic system is necessary for the learning.

Conversely, if persistent activity of DRN neurons acts as a substrate for the learning effect, activation of these neurons during the delay period should lead to extra attenuation of locomotor drive in the test period. To test this, we used two-photon optogenetic stimulation targeted to a small area of the DRN containing the serotonergic population (Figure 6E) in a fish expressing the ReaChR light-gated channel (Lin et al., 2013) in almost all neurons (*Tg(elavl3:ReaChR-TagRFP-T)*^{if10}) (Figures 6E and S7A). The light pulses were delivered either in the training period or in the delay period (Figures 6F and S7A–S7D). Stimulation of DRN neurons in the training period lowered the instantaneous locomotor drive (Figure 6G), showing that DRN activity is sufficient to attenuate ongoing locomotor drive, also consistent with the observation that two-photon DRN ablation increases locomotor drive (Figures S7E and S7F). This effect lasted less than 10 s (Figure 6H), i.e., the effect of artificial activation on the learning effect is briefer than that of behavioral training. Importantly, stimulation during the delay period significantly lowered the locomotor drive in the subsequent test period (Figure 6H), suggesting that optogenetic stimulation increases the level of the persistent DRN activity that encodes the learning effect and showing that DRN activity can adapt future behavior. Both of these effects were not observed when we stimulated a different area of the hindbrain in identical conditions in the same set of fish (Figure S7D).

We also selectively stimulated only serotonergic neurons in the DRN by scanning the two-photon laser only over individual serotonergic cells in fish co-expressing ReaChR in most neurons and GFP in serotonergic cells, *Tg(elavl3:ReaChR-TagRFP-T; pet1:GFP)* (Rickgauer and Tank, 2009). This stimulation also lowered future locomotor drive, for at least 3 s (Figures S7G and S7H). These pharmacologic, ablation, and area- and cell-type-specific optogenetics results support the hypothesis that the persistent activity of DRN serotonergic neurons during the delay period mediates the learning effect.

A Minimal DRN Model Exhibits Persistent Effects of Motor Adaptation

Our results provide preliminary support for a model in which the DRN integrates motor-gated visual feedback over multiple swim bouts to establish persistent activity that modulates locomotor drive for extended periods of time, thereby adapting behavior to changes in motosensory gain. To test whether such a hypothetical mechanism works in simulation, we amalgamated our observations of DRN function into a minimal model capturing our experimental observations (Figure 7A). In this model, the DRN, represented by a single variable capturing population

(H) Linear model fit to predict response amplitude from swim power and visual input confirms that average responses of serotonergic group 1 neurons are primarily tuned to visual stimulus velocity and less to locomotor drive as in Figures 2E and 2F and consistent with the response profile in (G). **p = 0.0014 by one-sample t test, 11 fish. Error bars: SEM across fish.

(I) Responses of an example GABAergic motor-type neuron by (left) dependence on visual velocity by motor-clamped analysis as in Figure 2E and (right) dependence on locomotor drive by visual-clamped analysis as in Figure 2F.

(J) Fitting a linear model as in (H) confirms that average responses of GABAergic motor-type neurons are primarily tuned to locomotor drive and less to visual stimulus velocity, consistent with response profile in (I). **p = 0.0052 by one-sample t test, eight fish. Error bars: SEM across fish.

See also Figure S5.

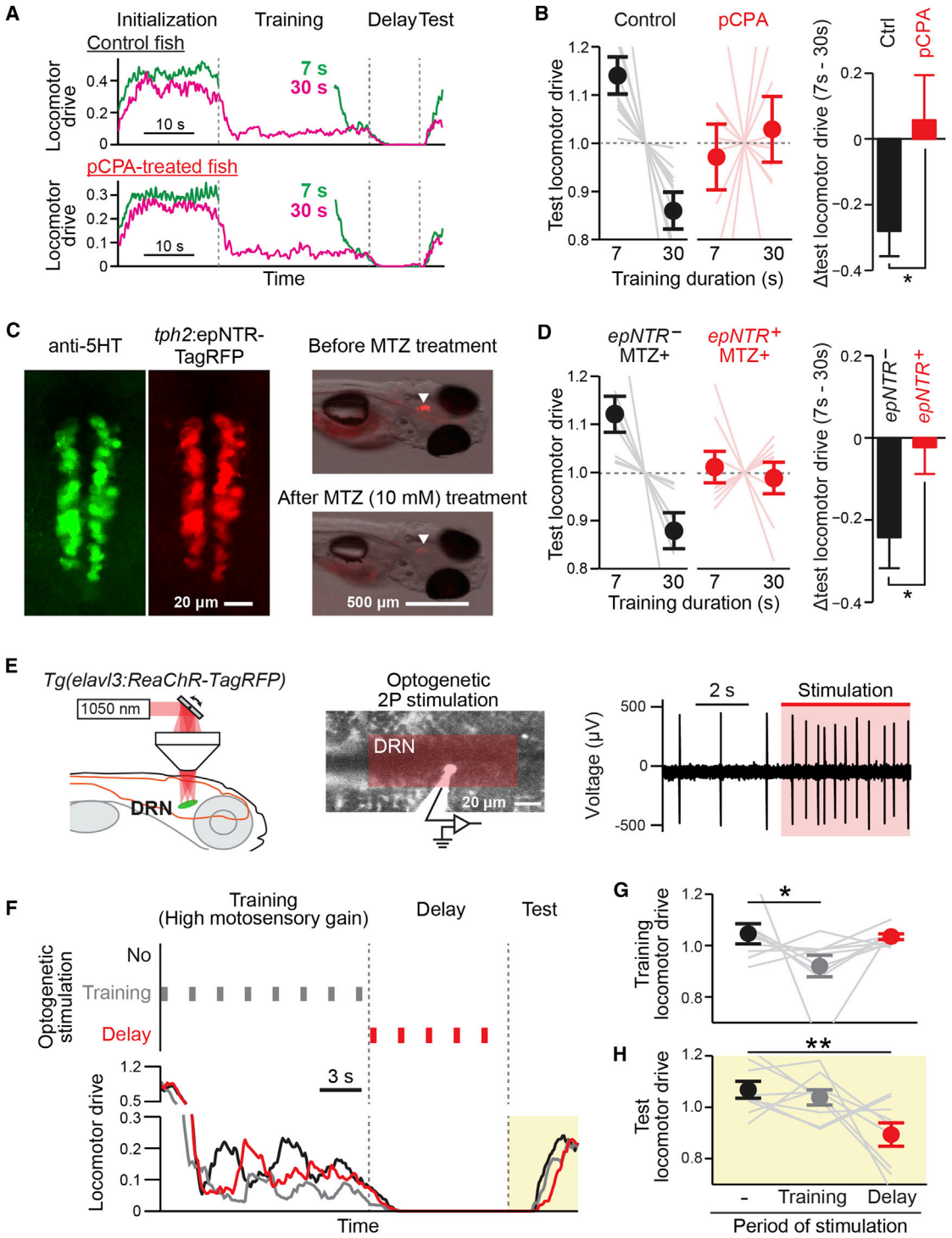

Figure 6. Serotonin Transmission and the DRN Are Causally Related to Learning

(A and B) Effects of pCPA serotonin release block on the learning effect. (A) Behavioral trace of control (top) and pCPA-treated (bottom) fish during the motor learning paradigm. (B) pCPA treatment leads to a loss of the learning effect. Left: test locomotor drive (integrated locomotor drive in the test period, normalized by the average across training conditions) is attenuated by longer training in the control group (black), but not in the pCPA-treated group (red). Faint lines, data from individual fish. Right: differences between test locomotor drive after short (7 s) or long (30) training durations. *p = 0.017 by Wilcoxon rank-sum test between ten control fish and ten pCPA-treated fish. Error bars, SEM across fish.

(legend continued on next page)

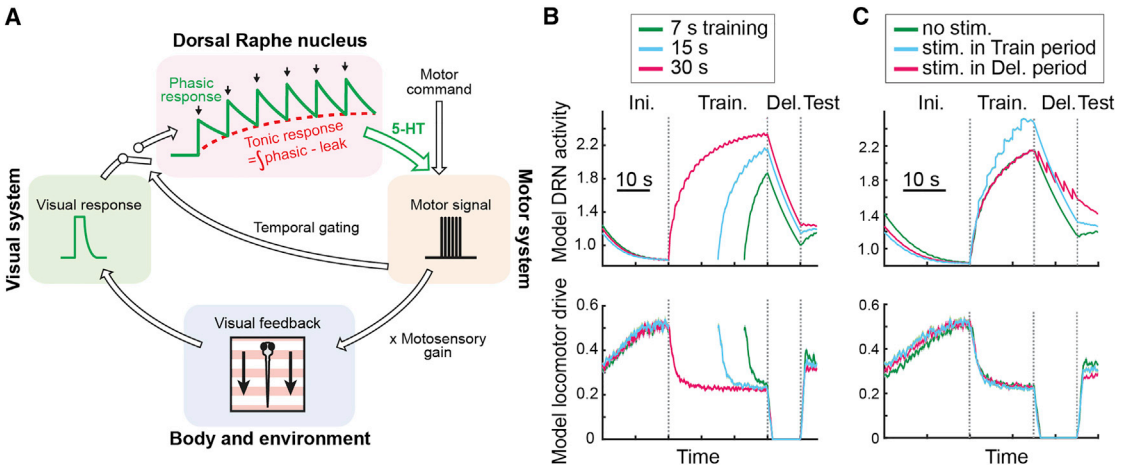

Figure 7. Minimal Model for Short-Term Locomotor Learning

(A) Model schematic. Simulated motor commands drive visual flow that depends on motosensory gain. The model DRN is a linear integrator with a slow decay time constant (15 s) that is phasically activated by visual flow during swim bouts. Due to slow decay dynamics, these phasic responses integrate and lead to motosensory-gain-dependent persistent DRN firing. This DRN firing then attenuates locomotor drive through nonlinear suppression.

(B) Behavior of the model in the motor learning paradigm. Top: model DRN activity averaged over 20 simulated trials is qualitatively similar to DRN activity in real experiments (Figure 4). Bottom: Locomotor drive increases during low motosensory gain, decreases during high gain, and exhibits the learning effect in the test period, similar to the behavior of real fish (Figure 1).

(C) Behavior of the model during simulation of the optogenetics experiment. Stimulation at 0.5 Hz during training slightly decreases locomotor drive in the training and test periods compared to no stimulation. Stimulation in the delay period decreases locomotor drive in test period.

activity, is a one-dimensional leaky integrator that integrates motor-gated visual feedback (Figures 2 and 3) over multiple swim bouts, has slow decay dynamics (Figure 4), and has a suppressive but saturating effect on motor output (Figures 6G and 6H). These three model components are sufficient to reproduce the qualitative features of the learning effect at the behavioral and neural levels (Figure 7B). The model also reproduces the main effects of optogenetic stimulation, where the effect of DRN activation is to suppress both instantaneous and future locomotor drive (Figure 7C).

DISCUSSION

The success of behaviors depends on executing the correct motor commands to achieve a desired effect, but the relationship between motor commands in the brain and the trajectory of the body is subject to ever-changing properties of the body and the environment. Here, we identified a functional implementation of a computation that detects the amount of displacement resulting from swim commands, forms a persistent representation of the effectiveness of motor commands in driving the fish forward, and modulates future locomotor drive to compensate for changes in motosensory gain. We found that this form of motor learning is mediated by the serotonergic system, which has not been traditionally associated with motor learning. Critical to this discovery was the ability to monitor activity across the entire brain of larval zebrafish engaged in short-term motor learning, because the brain areas mediating the learning were hitherto unknown.

There is a distinction between immediately observable behavioral adaptation (i.e., "real-time adaptation," which biases

(C and D) Effect of chemical-genetic ablation of *tph2*$^+$ serotonergic neurons on motor learning. (C) Left: 5-HT immunostaining (green) and nitroreductase (epNTR) expression in a *Tg(tph2:epNTR-RFP)* fish (red) in the DRN. Right: epNTR-TagRFP expression in the DRN (arrowhead) taken before (top, 4 dpf) and after (bottom, 6 dpf) metronidazole (MTZ) treatment for the same fish, fluorescence overlaid on bright field images. Most DRN neurons disappear. (D) Chemical genetic ablation leads to loss of the learning effect. Left: locomotor drive in the test period is attenuated by longer training in epNTR$^-$ siblings (black), but not in epNTR$^+$ group (red) after MTZ treatment. Faint lines, data from individual fish. Right: differences between test locomotor drive after short (7 s) and long (30 s) training. *p = 0.046 by Wilcoxon rank-sum test between eight epNTR$^-$ fish and nine epNTR$^+$ fish. Error bars, SEM across fish.

(E) Two-photon optogenetic activation of DRN neurons. Left: DRN neurons are specifically activated by laser scanning over a plane within the DRN. Center: location of a DRN neuron recorded by loose patch and electroporated with dye after recording. Red box, scan area. Right: raw recorded trace before and during optogenetic activation (red shadow) showing that the laser elicits extra spikes.

(F) Instantaneous effects of DRN activity on locomotor drive tested by stimulation during training (gray vertical lines and behavioral trace). Lasting effects were tested by stimulating in the delay period (red).

(G) DRN stimulation suppresses ongoing locomotor drive. Training locomotor drive is the integrated drive in the training period, normalized to the average across three stimulation conditions. p = 0.027 by one-way ANOVA. *p = 0.038 by Tukey's post hoc test. Error bars, SEM, nine fish. Gray dotted lines, data from individual fish.

(H) DRN stimulation in the delay period attenuates drive in the subsequent test period. This effect bridges the gap of ~3 s between the last stimulation pulse and the first swim bout in the test period. p = 0.0055 by one-way ANOVA. **p = 0.0069 by Tukey's post hoc test between delay stimulation and no stimulation for same nine fish as (G). Error bars, SEM across fish. Gray dotted lines, data from individual fish.

See also Figures S6 and S7.

current behavior in a useful manner) and the slower buildup of the more persistent effects of training (i.e., "learning," which biases future behavior in a useful manner despite intervening periods of disuse). When the DRN is ablated or serotonin release is blocked, real-time adaptation is still present (Figure S6) but the persistent effects are impaired (Figures 6A–6D). The real-time adaptation must therefore be driven, in part, by circuits outside the DRN.

Multiple forms of motor learning have been found to be mediated by the cerebellum (Raymond et al., 1996), which leads to the question why the form of locomotor learning studied here is mediated by the DRN. Although analogs exist between zebrafish locomotor learning and cerebellar learning such as in the vestibulo-ocular reflex (VOR) (Gao et al., 2012; Raymond et al., 1996), differences include the motor and sensory systems involved, the species, and the timescales of learning and memory. That said, interactions between cerebellar and raphe circuits exist (Pollak Dorocic et al., 2014; Weiss and Pellet, 1982; Weissbourd et al., 2014), and the role of the cerebellum in the current form of locomotor learning remains to be investigated. Indeed, although we identified an important component of adaptive motor control that either performs or reflects the integration of sensory outcomes, there may be circuits outside the DRN that partake in the integration process that were not detected due to limitations of the calcium indicator.

The observation of both phasic and persistent signals in the same neurons provides support for a model in which motor gating of sensory information yields motor-outcome-specific signals that the DRN integrates over time and communicates through serotonin release. This effectively computes a temporal running average of the velocity consequences of swim commands, to be used to modulate future locomotor drive. Integration may arise from single-cell mechanisms or from recurrent network effects that have previously been proposed to underlie working memory (Machens et al., 2005; Major and Tank, 2004; Miri et al., 2011). In addition to the effects of persistent DRN activity on behavior, the downstream effects of serotonin may add some additional persistence through the prolonged action of certain metabotropic serotonin receptors (Andrade et al., 1986).

The demonstration that the DRN mediates motor learning bears relation to prior work suggestive of a direct role for the serotonergic system in motor control. The DRN has been shown to encode motor and visual signals in cats and rodents (Jacobs and Fornal, 1997; Ranade and Mainen, 2009), and serotonin has been shown to affect movement gain in the spinal cord in humans (Wei et al., 2014) and regulate behavioral suppression (Soubrié, 1986). Serotonin also affects motor-related activity in invertebrates. For example, it can modulate motor patterns in the crab stomatogastric ganglion (Grashow et al., 2009) and mediate switches in locomotive states from roaming to dwelling in *Caenorhabditis elegans* (Flavell et al., 2013).

The DRN may change locomotor drive by directly modulating premotor centers, which may include reticulospinal neurons in the hindbrain or in the nucleus of the medial longitudinal fasciculus (McLean and Fetcho, 2004; Severi et al., 2014; Vertes and Linley, 2008). Serotonin may reduce the excitability of such premotor circuits, as serotonin from non-dorsal raphe nuclei can suppress locomotor rhythms in the spinal cord through activation of 5-HT_{1A} receptors in motor neurons or excitation of inhibitory interneurons (Cotel et al., 2013; Gabriel et al., 2009). The possibility that the DRN may directly modulate motor systems is supported by our finding that the learning effect generalizes between the forward OMR, the sideways OMR, and responses to darkening stimuli, and training does not change the reaction time or the probability of responding. A potential ethological reason for the generalization across stimulus conditions is that changes in temperature, viscosity, or energetic state will affect the motosensory gain similarly regardless of which stimulus triggered the swim response.

The central serotonergic system has been implicated in a wide range of processes, including value representation in associative learning (Amo et al., 2014 [median raphe]; Cohen et al., 2015; Dayan and Huys, 2015; Liu et al., 2014; Nakamura et al., 2008), patience (Fonseca et al., 2015; Miyazaki et al., 2014), feeding state (Filosa et al., 2016), sensory adaptation (Pantoja et al., 2016) and sensory responsiveness (Kapoor et al., 2016; Yokogawa et al., 2012), learned helplessness (Maier, 1984) and response to behavioral challenge (Warden et al., 2012), and mood regulation (Matthews and Harrison, 2012). The DRN computation revealed by the present work suggests possible relationships to prior work. In mice during associative learning, phasic DRN responses code for reward cues and punishments on individual trials and tonic firing codes for longer-term reward levels (Cohen et al., 2015), potentially analogous to the present observation of phasic signaling for visual feedback during individual swim bouts and tonic signaling for the learned longer-term motor effectiveness. Further, in rats, DRN activity has been found to influence how much an animal acts in the face of behavioral challenge (Warden et al., 2012); such behavioral choices are likely informed by internal estimates of action effectiveness. Where the DRN of larval zebrafish conveys the ease with which motor commands drive the fish forward, analogous representations of learned action effectiveness, potentially for multiple behaviors concurrently, might exist in other species. Uncovering the relationships between the computations carried out by the DRN across behavioral contexts may deliver unifying insights into the functions of the central serotonergic system.

STAR★METHODS

Detailed methods are provided in the online version of this paper and include the following:

- KEY RESOURCES TABLE
- CONTACT FOR REAGENTS AND RESOURCE SHARING
- EXPERIMENTAL MODEL AND SUBJECT DETAILS
  - Transgenic Zebrafish
- METHOD DETAILS
  - Preparation of Zebrafish for Fictive Behavior and Imaging Experiments
  - Behavioral Assays for Motor Learning in Virtual Reality
  - Comparison of Fictive and Free Swimming Behavior
  - Acquisition of Light-Sheet Imaging Data
  - High-Speed Calcium Imaging of Individual Brain Regions
  - Cell-Type Specific Imaging of *tph2*+ or *gad1b*+ Neurons in the DRN

SUPPLEMENTAL INFORMATION

Supplemental Information includes seven figures and one movie and can be found with this article online at http://dx.doi.org/10.1016/j.cell.2016.09.055.

A video abstract is available at http://dx.doi.org/10.1016/j.cell.2016.09.055#mmc2.

AUTHOR CONTRIBUTIONS

T.K. and M.B.A. conceived of the project and designed the experiments and analyses. T.K. carried out the experiments and the analyses. M.F.Z. performed the darkening probe experiments. B.D.M. and M.B.A. constructed the model. C.-T.Y. generated the *Tg(elavl3:H2B-GCaMP6f)*^{jf7} and *Tg(elavl3:ReaChR-TagRFP-T)*^{jf10} fish lines. T.K. generated the *Tg(tph2:epNTR-RFP)*^{jf41} fish line. T.K., B.D.M., and M.B.A. wrote the manuscript.

ACKNOWLEDGMENTS

We thank J. Freeman and J. Wittenbach for advice on data analyses; Y. Mu for collecting the freely swimming behavioral data; N. Vladimirov, P. Keller, M. Koyama and S. Narayan for discussions and technical assistance; H. Burgess, S. Higashijima and L. Bally-Cuif for sharing transgenic zebrafish; L. Looger and the Janelia GENIE project for providing calcium indicators; M. Barbic, T. Harris and the Janelia APIG group for technical assistance; R. Tsien for providing the ReaChR construct; J. Kuhl and E. Naumann for help with graphical illustrations; the Janelia Vivarium staff for fish care; N. Spruston, H. Lester, P. Dayan and M. Warden for discussions; and A. Bolton, M. Cembrowski, C. De Zeeuw, F. Engert, A. Hantman, D. Hildebrand, V. Jayaraman, M. Nonaka, J. Phillips, D. Stern, S. Sternson, K. Svoboda, M. Zlatic, and C. Zuker for advice on the manuscript. This study was supported by the Howard Hughes Medical Institute and by the Simons Foundation award 325171.

Received: January 20, 2016
Revised: July 21, 2016
Accepted: September 28, 2016
Published: October 27, 2016

REFERENCES

Ahrens, M.B., Li, J.M., Orger, M.B., Robson, D.N., Schier, A.F., Engert, F., and Portugues, R. (2012). Brain-wide neuronal dynamics during motor adaptation in zebrafish. Nature *485*, 471–477.

Amo, R., Fredes, F., Kinoshita, M., Aoki, R., Aizawa, H., Agetsuma, M., Aoki, T., Shiraki, T., Kakinuma, H., Matsuda, M., et al. (2014). The habenulo-raphe serotonergic circuit encodes an aversive expectation value essential for adaptive active avoidance of danger. Neuron *84*, 1034–1048.

Andalman, A.S., and Fee, M.S. (2009). A basal ganglia-forebrain circuit in the songbird biases motor output to avoid vocal errors. Proc. Natl. Acad. Sci. USA *106*, 12518–12523.

Andrade, R., Malenka, R.C., and Nicoll, R.A. (1986). A G protein couples serotonin and GABAB receptors to the same channels in hippocampus. Science *234*, 1261–1265.

Borue, X., Cooper, S., Hirsh, J., Condron, B., and Venton, B.J. (2009). Quantitative evaluation of serotonin release and clearance in Drosophila. J. Neurosci. Methods *179*, 300–308.

Boyden, E.S., Katoh, A., and Raymond, J.L. (2004). Cerebellum-dependent learning: the role of multiple plasticity mechanisms. Annu. Rev. Neurosci. *27*, 581–609.

Burgess, H.A., and Granato, M. (2007). Modulation of locomotor activity in larval zebrafish during light adaptation. J. Exp. Biol. *210*, 2526–2539.

Chen, T.-W., Wardill, T.J., Sun, Y., Pulver, S.R., Renninger, S.L., Baohan, A., Schreiter, E.R., Kerr, R.A., Orger, M.B., Jayaraman, V., et al. (2013). Ultrasensitive fluorescent proteins for imaging neuronal activity. Nature *499*, 295–300.

Cohen, J.Y., Amoroso, M.W., and Uchida, N. (2015). Serotonergic neurons signal reward and punishment on multiple timescales. eLife *4*. http://dx.doi.org/10.7554/eLife.06346.

Cotel, F., Exley, R., Cragg, S.J., and Perrier, J.-F. (2013). Serotonin spillover onto the axon initial segment of motoneurons induces central fatigue by inhibiting action potential initiation. Proc. Natl. Acad. Sci. USA *110*, 4774–4779.

Dayan, P., and Huys, Q. (2015). Serotonin's many meanings elude simple theories. eLife *4*, e07390.

Dunn, T.W., Mu, Y., Narayan, S., Randlett, O., Naumann, E.A., Yang, C.-T., Schier, A.F., Freeman, J., Engert, F., and Ahrens, M.B. (2016). Brain-wide mapping of neural activity controlling zebrafish exploratory locomotion. eLife *5*, e12741.

Filosa, A., Barker, A.J., Dal Maschio, M., and Baier, H. (2016). Feeding state modulates behavioral choice and processing of prey stimuli in the zebrafish tectum. Neuron *90*, 596–608.

Flavell, S.W., Pokala, N., Macosko, E.Z., Albrecht, D.R., Larsch, J., and Bargmann, C.I. (2013). Serotonin and the neuropeptide PDF initiate and extend opposing behavioral states in C. elegans. Cell *154*, 1023–1035.

Fonseca, M.S., Murakami, M., and Mainen, Z.F. (2015). Activation of dorsal raphe serotonergic neurons promotes waiting but is not reinforcing. Curr. Biol. *25*, 306–315.

Freeman, J., Vladimirov, N., Kawashima, T., Mu, Y., Sofroniew, N.J., Bennett, D.V., Rosen, J., Yang, C.-T., Looger, L.L., and Ahrens, M.B. (2014). Mapping brain activity at scale with cluster computing. Nat. Methods *11*, 941–950.

Gabriel, J.P., Mahmood, R., Kyriakatos, A., Söll, I., Hauptmann, G., Calabrese, R.L., and El Manira, A. (2009). Serotonergic modulation of locomotion in zebrafish: endogenous release and synaptic mechanisms. J. Neurosci. *29*, 10387–10395.

Gao, Z., van Beugen, B.J., and De Zeeuw, C.I. (2012). Distributed synergistic plasticity and cerebellar learning. Nat. Rev. Neurosci. *13*, 619–635.

Grashow, R., Brookings, T., and Marder, E. (2009). Reliable neuromodulation from circuits with variable underlying structure. Proc. Natl. Acad. Sci. USA *106*, 11742–11746.

Jacobs, B.L., and Fornal, C.A. (1997). Serotonin and motor activity. Curr. Opin. Neurobiol. *7*, 820–825.

Kapoor, V., Provost, A.C., Agarwal, P., and Murthy, V.N. (2016). Activation of raphe nuclei triggers rapid and distinct effects on parallel olfactory bulb output channels. Nat. Neurosci. *19*, 271–282.

Kawai, R., Markman, T., Poddar, R., Ko, R., Fantana, A.L., Dhawale, A.K., Kampff, A.R., and Ölveczky, B.P. (2015). Motor cortex is required for learning but not for executing a motor skill. Neuron *86*, 800–812.

Lillesaar, C., Stigloher, C., Tannhäuser, B., Wullimann, M.F., and Bally-Cuif, L. (2009). Axonal projections originating from raphe serotonergic neurons in the developing and adult zebrafish, Danio rerio, using transgenics to visualize raphe-specific pet1 expression. J. Comp. Neurol. *512*, 158–182.

Lin, J.Y., Knutsen, P.M., Muller, A., Kleinfeld, D., and Tsien, R.Y. (2013). ReaChR: a red-shifted variant of channelrhodopsin enables deep transcranial optogenetic excitation. Nat. Neurosci. *16*, 1499–1508.

Lister, J.A., Robertson, C.P., Lepage, T., Johnson, S.L., and Raible, D.W. (1999). nacre encodes a zebrafish microphthalmia-related protein that regulates neural-crest-derived pigment cell fate. Development *126*, 3757–3767.

Liu, Z., Zhou, J., Li, Y., Hu, F., Lu, Y., Ma, M., Feng, Q., Zhang, J.E., Wang, D., Zeng, J., et al. (2014). Dorsal raphe neurons signal reward through 5-HT and glutamate. Neuron *81*, 1360–1374.

Machens, C.K., Romo, R., and Brody, C.D. (2005). Flexible control of mutual inhibition: a neural model of two-interval discrimination. Science *307*, 1121–1124.

Maier, S.F. (1984). Learned helplessness and animal models of depression. Prog. Neuropsychopharmacol. Biol. Psychiatry *8*, 435–446.

Major, G., and Tank, D. (2004). Persistent neural activity: prevalence and mechanisms. Curr. Opin. Neurobiol. *14*, 675–684.

Masino, M.A., and Fetcho, J.R. (2005). Fictive swimming motor patterns in wild type and mutant larval zebrafish. J. Neurophysiol. *93*, 3177–3188.

Matthews, P.R., and Harrison, P.J. (2012). A morphometric, immunohistochemical, and in situ hybridization study of the dorsal raphe nucleus in major depression, bipolar disorder, schizophrenia, and suicide. J. Affect. Disord. *137*, 125–134.

McLean, D.L., and Fetcho, J.R. (2004). Relationship of tyrosine hydroxylase and serotonin immunoreactivity to sensorimotor circuitry in larval zebrafish. J. Comp. Neurol. *480*, 57–71.

Miri, A., Daie, K., Arrenberg, A.B., Baier, H., Aksay, E., and Tank, D.W. (2011). Spatial gradients and multidimensional dynamics in a neural integrator circuit. Nat. Neurosci. *14*, 1150–1159.

Miyazaki, K.W., Miyazaki, K., Tanaka, K.F., Yamanaka, A., Takahashi, A., Tabuchi, S., and Doya, K. (2014). Optogenetic activation of dorsal raphe serotonin neurons enhances patience for future rewards. Curr. Biol. *24*, 2033–2040.

Morton, S.M., and Bastian, A.J. (2006). Cerebellar contributions to locomotor adaptations during splitbelt treadmill walking. J. Neurosci. *26*, 9107–9116.

Nakamura, K., Matsumoto, M., and Hikosaka, O. (2008). Reward-dependent modulation of neuronal activity in the primate dorsal raphe nucleus. J. Neurosci. *28*, 5331–5343.

Niell, C.M., and Stryker, M.P. (2010). Modulation of visual responses by behavioral state in mouse visual cortex. Neuron *65*, 472–479.

Orger, M.B., Kampff, A.R., Severi, K.E., Bollmann, J.H., and Engert, F. (2008). Control of visually guided behavior by distinct populations of spinal projection neurons. Nat. Neurosci. *11*, 327–333.

Panigrahi, B., Martin, K.A., Li, Y., Graves, A.R., Vollmer, A., Olson, L., Mensh, B.D., Karpova, A.Y., and Dudman, J.T. (2015). Dopamine is required for the neural representation and control of movement vigor. Cell *162*, 1418–1430.

Pantoja, C., Hoagland, A., Carroll, E.C., Karalis, V., Conner, A., and Isacoff, E.Y. (2016). Neuromodulatory regulation of behavioral individuality in zebrafish. Neuron *91*, 587–601.

Parker, M.O., Brock, A.J., Walton, R.T., and Brennan, C.H. (2013). The role of zebrafish (Danio rerio) in dissecting the genetics and neural circuits of executive function. Front. Neural Circuits *7*, 63.

Pollak Dorocic, I., Fürth, D., Xuan, Y., Johansson, Y., Pozzi, L., Silberberg, G., Carlén, M., and Meletis, K. (2014). A whole-brain atlas of inputs to serotonergic neurons of the dorsal and median raphe nuclei. Neuron *83*, 663–678.

Portugues, R., and Engert, F. (2011). Adaptive locomotor behavior in larval zebrafish. Front. Syst. Neurosci. *5*, 72.

Ranade, S.P., and Mainen, Z.F. (2009). Transient firing of dorsal raphe neurons encodes diverse and specific sensory, motor, and reward events. J. Neurophysiol. *102*, 3026–3037.

Randlett, O., Wee, C.L., Naumann, E.A., Nnaemeka, O., Schoppik, D., Fitzgerald, J.E., Portugues, R., Lacoste, A.M.B., Riegler, C., Engert, F., and Schier, A.F. (2015). Whole-brain activity mapping onto a zebrafish brain atlas. Nat. Methods *12*, 1039–1046.

Raymond, J.L., Lisberger, S.G., and Mauk, M.D. (1996). The cerebellum: a neuronal learning machine? Science *272*, 1126–1131.

Rickgauer, J.P., and Tank, D.W. (2009). Two-photon excitation of channelrhodopsin-2 at saturation. Proc. Natl. Acad. Sci. USA *106*, 15025–15030.

Ronneberger, O., Liu, K., Rath, M., Rueβ, D., Mueller, T., Skibbe, H., Drayer, B., Schmidt, T., Filippi, A., Nitschke, R., et al. (2012). ViBE-Z: a framework for 3D virtual colocalization analysis in zebrafish larval brains. Nat. Methods *9*, 735–742.

Satou, C., Kimura, Y., Hirata, H., Suster, M.L., Kawakami, K., and Higashijima, S. (2013). Transgenic tools to characterize neuronal properties of discrete populations of zebrafish neurons. Development *140*, 3927–3931.

Seelig, J.D., and Jayaraman, V. (2013). Feature detection and orientation tuning in the Drosophila central complex. Nature *503*, 262–266.

Severi, K.E., Portugues, R., Marques, J.C., O'Malley, D.M., Orger, M.B., and Engert, F. (2014). Neural control and modulation of swimming speed in the larval zebrafish. Neuron *83*, 692–707.

Smith, M.A., Ghazizadeh, A., and Shadmehr, R. (2006). Interacting adaptive processes with different timescales underlie short-term motor learning. PLoS Biol. *4*, e179.

Soubrié, P. (1986). Reconciling the role of central serotonin neurons in human and animal behavior. Behav. Brain Sci. *9*, 319–335.

Tabor, K.M., Bergeron, S.A., Horstick, E.J., Jordan, D.C., Aho, V., Porkka-Heiskanen, T., Haspel, G., and Burgess, H.A. (2014). Direct activation of the Mauthner cell by electric field pulses drives ultrarapid escape responses. J. Neurophysiol. *112*, 834–844.

Vertes, R., and Linley, S. (2008). Efferent and afferent connections of the dorsal and median raphe nuclei in the rat. In Serotonin and Sleep: Molecular, Functional and Clinical Aspects, J.M. Monti, S.R. Pandi-Perumal, B.L. Jacobs, and D.J. Nutt, eds. (Birkhäuser Verlag), pp. 69–102.

Vladimirov, N., Mu, Y., Kawashima, T., Bennett, D.V., Yang, C.-T., Looger, L.L., Keller, P.J., Freeman, J., and Ahrens, M.B. (2014). Light-sheet functional imaging in fictively behaving zebrafish. Nat. Methods *11*, 883–884.

Warden, M.R., Selimbeyoglu, A., Mirzabekov, J.J., Lo, M., Thompson, K.R., Kim, S.-Y., Adhikari, A., Tye, K.M., Frank, L.M., and Deisseroth, K. (2012). A prefrontal cortex-brainstem neuronal projection that controls response to behavioural challenge. Nature *492*, 428–432.

Wei, K., Glaser, J.I., Deng, L., Thompson, C.K., Stevenson, I.H., Wang, Q., Hornby, T.G., Heckman, C.J., and Kording, K.P. (2014). Serotonin affects movement gain control in the spinal cord. J. Neurosci. *34*, 12690–12700.

Weiss, M., and Pellet, J. (1982). Raphe - cerebellum interactions. I. Effects of cerebellar stimulation and harmaline administration on single unit activity of midbrain raphe neurons in the rat. Exp. Brain Res. *48*, 163–170.

Weissbourd, B., Ren, J., DeLoach, K.E., Guenthner, C.J., Miyamichi, K., and Luo, L. (2014). Presynaptic partners of dorsal raphe serotonergic and GABAergic neurons. Neuron *83*, 645–662.

Yin, H.H., Mulcare, S.P., Hilário, M.R.F., Clouse, E., Holloway, T., Davis, M.I., Hansson, A.C., Lovinger, D.M., and Costa, R.M. (2009). Dynamic reorganization of striatal circuits during the acquisition and consolidation of a skill. Nat. Neurosci. *12*, 333–341.

Yokogawa, T., Hannan, M.C., and Burgess, H.A. (2012). The dorsal raphe modulates sensory responsiveness during arousal in zebrafish. J. Neurosci. *32*, 15205–15215.

STAR★METHODS

KEY RESOURCES TABLE

REAGENT or RESOURCE	SOURCE	IDENTIFIER
Antibodies		
anti-5-HT rabbit polyclonal antibody	Sigma-Aldrich	S5545; RRID: AB_477522
anti-rabbit secondary antibody conjugated with Cy3	Jackson ImmunoResearch	711-165-152; RRID: AB_2307443
anti-rabbit secondary antibody conjugated with Cy5	Jackson ImmunoResearch	711-175-152; RRID: AB_2340607
Alexa Fluor 594 hydrazide, sodium salt	Thermo Fisher Scientific	A10438
Chemicals for Pharmacology Assays, Paralysis, and Anesthesia		
Hoechst 33342	Life Technologies	H3570
Alpha-Bungarotoxin	Life Technologies	B1601
Tricaine	Sigma-Aldrich	A5040
Para-chlorophenylalanine (pCPA)	Tocris Bioscience	0938
Metronidazole	MP Biomedicals	02155710
DNA Materials		
epNTR-TagRFP	Tabor et al., 2014	N/A
tph2 promoter in Tol2 vector	Yokogawa et al., 2012	N/A
Transgenic Animals		
Tg(elavl3:H2B-GCaMP6f)^{jf7}	Dunn et al., 2016	N/A
Tg(elavl3:ReaChR-TagRFP-T)^{jf10}	Dunn et al., 2016	N/A
Tg(pet1:EGFP)^{ne0214Tg}	Lillesaar et al., 2009	N/A
Tg(gad1b:loxP-RFP-loxP-GFP)^{nns26Tg}	Satou et al., 2013	N/A
Tg(elavl3:GCaMP6f)^{jf1}	Dunn et al., 2016	N/A
Tg(tph2:epNTR-TagRFP)^{jf41}	Ahrens lab; ZIRC	N/A
Software		
MATLAB R2014a	Mathworks	http://www.mathworks.com/products/matlab/
CUDA	Nvidia Corporation	https://developer.nvidia.com/cuda-toolkit
SPM8	University College London	www.fil.ion.ucl.ac.uk/spm/software/spm8/
CUDA script for Image registration	Ahrens lab	https://github.com/ahrens-lab/Kawashima_et_al_Cell_2016/
MATLAB script for neuron detection	Ahrens lab	https://github.com/ahrens-lab/Kawashima_et_al_Cell_2016/
MATLAB script for calculating brain deformation	Ahrens lab	https://github.com/ahrens-lab/Kawashima_et_al_Cell_2016/

CONTACT FOR REAGENTS AND RESOURCE SHARING

Further information and requests for resources and reagents should be directed to the corresponding author Misha Ahrens (ahrensm@janelia.hhmi.org).

EXPERIMENTAL MODEL AND SUBJECT DETAILS

All experiments presented in this study were conducted according to the animal research guidelines from NIH and were approved by the Institutional Animal Care and Use Committee and Institutional Biosafety Committee of Janelia Research Campus.

Transgenic Zebrafish

All experiments in this study were performed on larval zebrafish 5 or 6 d.p.f. (days post fertilization) in the *nacre* background (Lister et al., 1999). The transgenic lines *Tg(elavl3:H2B-GCaMP6f)*^{jf7} and *Tg(elavl3:ReaChR- TagRFP-T)*^{jf10} have been previously described (Dunn et al., 2016). *Tg(pet1:EGFP)*^{ne0214Tg} (Lillesaar et al., 2009) and *Tg(gad1b:loxP-RFP-loxP-GFP)*^{nns26Tg} (Satou et al., 2013) were

generous gifts from Dr. Laure Bally-Cuif and Dr. Shin-ichi Higashijima, respectively. We generated the *Tg(elavl3:GCaMP6f)*^{jf1} line and the *Tg(tph2:epNTR-TagRFP)*^{jf41} line using the Tol2 transposon system. For the latter, epNTR-TagRFP (Tabor et al., 2014) was fused to *tph2* promoter (Yokogawa et al., 2012) in a Tol2 vector. The DNA and transposase mRNAs were injected in 2-cell stage embryos and the expression of red fluorescence in the brain was screened for transgenesis at the F1 generation. The fish lines are available upon request.

METHOD DETAILS

Preparation of Zebrafish for Fictive Behavior and Imaging Experiments

The system for performing whole-brain light-sheet imaging in zebrafish behaving fictively in a virtual environment was implemented as described before (Vladimirov et al., 2014). Briefly, 5-6 d.p.f. larval zebrafish were immobilized by bath application of α-Bungarotoxin (1mg/ml) dissolved in external solution (in mM: 134 NaCl, 2.9 KCl, 2.1 $CaCl_2$, 1.2 $MgCl_2$, 10 HEPES, 10 glucose [pH 7.8]; 290 mOsm) for 25-50 s and embedded in agarose on a custom-made pedestal inside a glass-walled chamber with a diffusive screen underneath the fish (pedestal design is available as an STL file for 3D printing). Agarose around the head was removed to minimize scattering of the excitation later. Laser power at the head was on average approximately 44 μW (with a 12 ms laser sweep at 66 μW followed by a 6 ms period of no light for each 18 ms image exposure). The distance between the fish and the display was about 4 mm. Electric signals from motor neuron axons in the tail were recorded using borosilicate pipettes (TW150-3, World Precision Instruments) pulled by a vertical puller (PC-10, Narishige) and shaped by a microforge (MF-900, Narishige). The pipettes were filled with fish rearing water and connected to the tail using minimal negative pressure. Swim signals were recorded using an amplifier (MultiClamp 700B, Molecular Devices).

Behavioral Assays for Motor Learning in Virtual Reality

We simulated an environment in which the animals swim along a one-dimensional virtual track consisting of red and black bars (each 2 mm thick) perpendicular to the direction of swimming (Figure 1A) as previously described (Ahrens et al., 2012). The visual effect of swimming was mimicked by accelerating the gratings backward when a fictive swim bout was detected (Figure 1B). We simulated an environment in which fish swim against a virtual water current, so that in between swim bouts, the visual environment slowly moved forward at 2 mm/s (Figure 1B), to visually simulate backward movement of the fish due to the virtual backward water flow. The purpose of this virtual water current was to increase the baseline rate of swim events, because forward whole-field motion elicits swim bouts (the forward optomotor response or OMR; the function of this behavior is presumably to stabilize the position of the fish in the presence of water flow). Thus the forward velocity of the gratings is [forward visual flow velocity] = [forward offset velocity] – [locomotor drive] × [motosensory gain] (Figures 1B and 1C). During strong enough swim bouts, this value becomes negative, i.e., the visual environment moves backward simulating forward swimming, allowing the fish to stabilize the position of the visual environment over time. The motosensory gain is a parameter describing the amount of backward motion arising from swimming (i.e., simulated forward movement of the fish), and simulates factors such as the viscosity of the water, the temperature of the muscles and the metabolic state of the animal. In all experiments with multiple motosensory gain levels, 'low motosensory gain' was chosen to be slightly higher than the minimal possible value of motosensory gain at which the fish could still keep up with the gratings; 'medium motosensory gain' was set to 2 times that value, and 'high motosensory gain' was set to 3 times that value.

The behavioral assay for testing the learning effect is illustrated in Figures 1D and 1E. The paradigm consisted of low-gain initialization periods, high-gain training periods, delay periods, and medium-gain test periods. In the delay period, the fish was presented with slowly backward moving gratings (0.8 mm/s) for most of the experiments (Figures 1, 4A–4E, 5A–5F, 6, and S7H). In other experiments (Figures 4F, S1A, and S1D–S1I), a white screen was instead presented during the delay period because in some cases this better suppressed spontaneous swimming (Figures 4F and S1A) and better triggered swim responses to sideways-moving gratings or darkening stimuli in the next test period (Figures S1D and S1G). We collected between 30 and 40 trials of the same task per experiment, where one trial consists of [20 s of low motosensory gain period] [either 7, 15 or 30 s of high motosensory gain period] [10 s of delay period] [5 s of test period] (labeled initialization-, training-, delay- and test periods). The strength of the learning effect depended on several factors including the luminosity of the stimulus in the delay period and a sufficiently low contrast of the moving visual stimulus, which we tuned over the course of several experiments to achieve the strongest learning effect.

In the experiments of Figures 2C–2F and 5G–5J, to equalize the magnitude of motor output in different gain conditions, the motosensory gain was changed semi-randomly for every swim bout as illustrated in Figure 2C. For the behavioral paradigm for desynchronizing swim events and visual feedback (Figure 3), the sequence of task periods is as follows, repeated 9 times: (1) 20 s of no visual motion (stop period), (2) 20 s of closed-loop under high motosensory gain (closed-loop period); the stimulus during this period is 'recorded' for replay later on, (3) 20 s of stop period, and (4) 20 s of 'replay' where the identical time-varying stimulus as the preceding closed-loop period is replayed in open-loop so that the fish has no control over it (replay period) (Figures 3B and S4F).

For the optogenetics experiment (Figures 6E–6H, S7G, and S7H) we used, instead of red-black moving gratings, blue-black gratings with identical parameters to prevent nonspecific activation of ReaChR channels. We confirmed that using the blue color channel of our projector to generate gratings also reliably elicited the OMR.

Fictive swim signals were acquired at 6 kHz using a MultiClamp 700B amplifier (Molecular Devices) and a National Instruments data acquisition board controlled by custom software (Ahrens et al., 2012) written in C# (Microsoft). Visual stimuli were delivered using a

LCD projector (M2, AAXA) or a laser projector (MP-CL1, Sony). In the light sheet experiments, the start of the different periods of the behavioral assay was synchronized to the microscope scans, which were performed either at 1.0 Hz (i.e., at one brain volume per second) (Figures 1, 4A, 4B, 4H, 5A–5F, S3B, S4B, and S5A–S5D) or at 30 Hz (Figures 2, 3, 5G–5J, S4D–S4F, S5E, and S5F).

Comparison of Fictive and Free Swimming Behavior

To compare properties of fictive swim bouts to those of freely swimming fish, we filmed freely swimming fish performing the OMR. To quantify the temporal patterns of freely swimming fish, individual larval zebrafish (5-7 d.p.f.) were filmed swimming in a petri dish above a screen showing moving gratings using a high-speed camera (Pike, Allied Vision) recording images at 30 Hz. Times of swim bouts for 21 fish were automatically detected using custom scripts written in MATLAB. Freely swimming fish swam at 1.44 ± 0.06 Hz in the optomotor response (n = 5 fish); fictively swimming fish swam at 1.19 ± 0.04 Hz under low motosensory gain (same fish as in Figure S1B, n = 12). Free swim bouts lasted 0.19 ± 0.01 s (n = 5); fictive swim bouts lasted 0.26 ± 0.02 s (n = 12). These results suggest that in the current assay the statistics of fictive behavior in the virtual track are qualitatively similar to those of freely swimming behavior.

Acquisition of Light-Sheet Imaging Data

Whole brain imaging using light-sheet microscopy in Figures 1H, 4, 5A–5F, S4B, and S5A–S5D was performed on volumes spanning 240 μm along the dorso-ventral axis (45 z-planes, 5.5 μm intervals) and extending 820 and 410 μm across the longitudinal and lateral axes in *Tg(elavl3:H2B-GCaMP6f)*^{jf7} fish which express GCaMP6f (Chen et al., 2013) in most neurons with the indicator localized to the nucleus. The imaging was performed using the system described in Vladimirov et al. (2014). Brain scans were made by using an orthogonal dual-laser setup that scanned almost the entire brain without shining the laser beams into the eyes of the fish. During image acquisition for 30-40 min, the acquired data were directly written to a SSD RAID hard drive. Subsequent analysis was performed as described in QUANTIFICATION AND STATISTICAL ANALYSIS.

High-Speed Calcium Imaging of Individual Brain Regions

High-speed calcium imaging of DRN neurons described in Figures 2, 3, 5G–5J, S4D–S4G, S5E, and S5F was performed using *Tg(elavl3:GCaMP6f)*^{jf1} fish which express GCaMP6f in the cytosol. A single plane of a narrow area around the DRN or in the optic tectum was imaged at 30Hz in the same light-sheet microscope setup as described above. In these datasets, neurons were identified manually. Subsequent analysis was performed as described in QUANTIFICATION AND STATISTICAL ANALYSIS.

Cell-Type Specific Imaging of *tph2*+ or *gad1b*+ Neurons in the DRN

For the analysis of activity patterns of *tph2*+ or *gad1b*+ neurons during the short-term motor learning paradigm in Figures 5A–5F, transgenic zebrafish expressing nuclear-localized GCaMP6f (*Tg(elavl3:H2B-GCaMP6f)*^{jf7}) were crossed to either *Tg(tph2:epNTR-TagRFP)*^{jf41} (for labeling *tph2*+ serotonergic neurons; the epNTR was not used in these experiments) or *Tg(gad1b:loxP-RFP-loxP-GFP)*^{nns26Tg} (for labeling *gad1b*+ GABAergic neurons) to produce double transgenic zebrafish. After neuronal activity across the whole brain was imaged and individual neurons' activity traces were extracted as explained in Figures S2A and S2B, analysis was performed as described in QUANTIFICATION AND STATISTICAL ANALYSIS.

For imaging fast activity dynamics of *tph2*+ or *gad1b*+ neurons in Figures 5G–5J, S5E, and S5F, transgenic zebrafish which express cytosolic GCaMP6f (*Tg(elavl3: GCaMP6f)*^{jf1}) were crossed with either *Tg(tph2:epNTR-TagRFP)*^{jf41} (for *tph2*+ serotonergic neurons) or *Tg(gad1b:loxP-RFP-loxP-GFP)*^{nns26Tg} (for *gad1b*+ GABAergic neurons) to produce double transgenic zebrafish. We imaged the activity of the same set of neurons in two different behavioral paradigms, the stochastic gain paradigm described in Figure 2 and the short-term motor learning paradigm described in Figure 1, so that we could examine the relationship between the fast sensorimotor encoding dynamics and the slow activity dynamics in the short-term motor learning task (Figures 5B and 5E). The analysis of these data is described in QUANTIFICATION AND STATISTICAL ANALYSIS.

Single-Cell Electrical Recordings

Single-cell loose-patch recordings were performed using *Tg(elavl3:H2B-GCaMP6f)*^{jf7} fish in a custom-built two-photon microscope equipped with the same virtual reality setup and a 25x objective lens (NA 0.95, Leica). Fire-polished borosilicate glass pipettes (BF150-75-7.5, Sutter) pulled by a horizontal puller (P1000, Sutter) were filled with external solution containing the red Alexa594 fluorescent dye and connected to a pressure controller (DPM1B, Fluke). The typical resistance of the recording pipette was between 9 and 10 MΩ. The fish was bathed in external solution, and a tiny skin incision was made between the border of the optic tectum and the cerebellum for pipette access. The movement of the recording pipette was controlled by a micromanipulator (MPC-265, Sutter) and was monitored with the two-photon microscope in the green and red channels with an excitation wavelength of 850 nm. Upon entry into the brain, positive pressure (15-30 mmHg) was applied to the pipette, and after cell attachment a small amount of negative pressure (< 2 mmHg) was applied. The signals were amplified by an electrophysiology amplifier (MultiClamp 700B, Molecular Devices), high-pass filtered at 100 Hz, and acquired at 6 kHz using a National Instruments DAQ board and software custom-written in C#. The recordings typically lasted between 10 and 30 min. Simultaneously, recordings were made from the motor neuron axons in the tail on the other side of the fish to monitor fictive swim signals used in the short-term motor learning paradigm. Spikes were reliably detected by thresholding the voltage trace offline (at 400-500 μV).

For Figure 4E, we removed from the analysis some trials in which a swim bout overlapped with the transition of the motosensory gain (from the initialization period to the training period) to avoid the effect of mixed feedback information on the subsequent swim events.

Two-Photon and Chemical-Genetic Ablations of DRN Neurons

Plasma-mediated two-photon ablations in Figure S7E were performed by applying brief, high-power (~200 mW under the objective) pulses of femtosecond infrared laser (Chameleon Ultra II, Coherent) through a 25x objective lens (NA 0.95, Leica) in the same two-photon microscope as described above. After opening the mechanical shutter (VS14, Vincent Associates), small spiral scans with a radius of 0.9 μm were applied to the centers of neurons until a plasma spark was detected by the photomultiplier (H10770PB-40, Hamamatsu) whereupon the shutter was automatically closed. The ablation typically took 125 to 500 ms per neuron. An interval of 2 s was set between shutter openings when multiple neurons were ablated. For DRN ablation, 40-50 neurons close to the midline were targeted across multiple Z planes (Figure S7E). Fish behavior was tested before ablation, and again after ablation following a recovery period of 10-20 min. The spatial extent and the efficiency of ablation was confirmed post hoc by intrabrain injection of propidium iodide (1.0 mg/mL, Life Technologies), a membrane impermeable dye that passes through disrupted membranes of dead cells and increases fluorescence when intercalated to nucleic acids (Figure S7E). This acute two-photon ablation of DRN neurons was not used for causality experiments for the short-term motor learning assay, because it caused an increased amount of spontaneous swimming during the delay period, which interfered with the behavioral evaluation of the learning effect.

For chemical-genetic ablation of DRN serotonergic neurons in Figures 6C, 6D and S6, both epNTR- and epNTR+ sibling fish were treated with 10 mM metronidazole (MP Biomedicals) dissolved in fish rearing water for 12 hr between 4 and 5 d.p.f. After being transferred to normal fish rearing water and fed with paramecia for more than 24 hr, the fish were subjected to behavioral tests to compare the lesioned and control groups at 6 d.p.f.

Pharmacology

Para-chlorophenylalanine (pCPA) is a potent serotonin synthesis inhibitor which is known to inhibit serotonin release within 30 min after bath application (Borue et al., 2009). pCPA was dissolved in fish rearing water at a concentration of 1 mM and applied to the fish by bath for 8-12 hr before testing the behavior at 6 d.p.f. Paralysis and behavioral testing was also performed in the presence of 1mM pCPA.

Optogenetic Experiments

In the two-photon optogenetic local activation experiments in Figures 6E–6H and S7A–S7D, the DRN or hindbrain neurons of *Tg(elavl3:ReaChR-TagRFP-T)*^{jf10} fish were stimulated by raster scanning a two-photon laser. The stimulation laser was set to a wavelength of 1050 nm and at a power of 50 mW under the objective. Two regions of interest (ROIs) were predefined: a 'target' ROI either over the raphe nucleus or over a control region in the hindbrain. Further, a 'null' ROI was defined outside the fish, so that the stimulation could be pulsed by rapidly switching between the ROI of interest and the null ROI using the galvanometer scanners. In the initialization period, the laser shutter was closed to avoid accumulation of heat around the fish during the experiment. Then the shutter was opened during the training, delay and test periods, and the galvo positions were switched between 'null' ROI and the 'target' ROI (in the DRN or control region), so that the 'target' ROI was stimulated for 200 ms once every 2 s. During stimulation, raster scanning was performed over the ROI at a frequency of 20 Hz, i.e., 4 raster scans per stimulation. Reliable excitation of neuronal spikes by laser scanning was verified using single-cell recording (Figure 6E).

In the cell-type-specific optogenetic activation experiments in Figures S7G and S7H, serotonergic neurons in the DRN were sequentially stimulated with a two-photon laser in double transgenic fish [*Tg(elavl3:ReaChR- TagRFP-T)*^{jf10} ; *Tg(pet1:EGFP)*^{ne0214Tg}]. The stimulation laser was set to a wavelength of 1050 nm and at a power of 50 mW under the objective, and 10 *pet1*+ neurons, marked by *pet1:GFP*, were sequentially scanned with 5 ms dwell time per cell. Within the 5 ms period, a spiral scan (Rickgauer and Tank, 2009) with a diameter of 3-4 μm was repeated 6 times (0.83 ms per circular scan; radius continually varying to create a spiral measuring from the edge of the outer circle to half-way toward the center) (Figure S7G). This sequential stimulation of 10 neurons (50 ms in total) was repeated 4 times (200 ms total), 2 s before the end of the delay period.

Immunohistochemistry

Whole-mount staining of zebrafish brains was performed as follows. The 6-d.p.f. larvae were anesthetized by bath application of 0.02% tricaine solution and then fixed by immersion in a 4% solution of paraformaldehyde in PBS at 4°C overnight. The next day, the brain tissue was isolated by manual dissection. The brain was treated with blocking solution [10% donkey serum, 0.8% Triton-X in PBS] at 4°C overnight, and then treated with an anti-5H-T rabbit polyclonal antibody (1:500, S5545, Sigma) in the blocking solution at 4°C for 3 days. After washing with PBS-T [0.8% Triton-X in PBS], the brain was further treated with an anti-rabbit secondary antibody conjugated with Cy3 or Cy5 (1:500, 711-165-152 / 711-175-152, Jackson ImmunoResearch) together with Hoechst 33342 (1:2000, H3570, Life Technologies) in the blocking solution at 4°C for 2 days. After washing with PBS-T, the brains were mounted on a cover glass and imaged with a confocal microscope (LSM780 or LSM880, Zeiss) or a custom-built two-photon microscope as described above.

Reduced Network Model of DRN Function and Motor Adaptation Behavior

We simulated the minimal model schematized in Figure 7 and described in the main text using MATLAB (Mathworks). DRN activity was simplified to a single variable, r, summarizing the population activity of the entire DRN. The DRN is modeled to be a leaky integrator of motor-gated visual flow, so that when visual flow, v, is present and the fish swims, r increases, and when no visual flow is present or the fish does not swim, r slowly decreases. In turn, r has a suppressive effect on locomotor drive, m. The model is simulated according to the equations below,

$$dr/dt = -1/\tau \times r + bv^2 \quad \text{when the fish swims} \tag{1a}$$

$$dr/dt = -1/\tau \times r \quad \text{when the fish does not swim} \tag{1b}$$

$$m = 1 + 1/r^{2.5} \quad \text{when the fish swims} \tag{2a}$$

$$m = 0 \quad \text{when the fish does not swim} \tag{2b}$$

$$v = m \times [\textit{motosensory gain}] \tag{3}$$

Here τ is the decay time constant of the DRN, which we set 15 s based on the imaging and electrophysiology data. Here b describes the strength of the motor-gated visual response of the DRN, which we set to 1/8. The model fish swims once every 1.5 s with 100 ms jitter in onset timing; swims are 300 ms in duration. The motosensory gain was 0.5, 1 or 2; and the timing of the assay was set as in the real short-term motor learning paradigm described in Figure 1D. Equation (1) models the DRN as a leaky integrator, based on the observation that activity decays slowly during the delay period, and that there is a phasic response to visual input, which we model as a motor-gated nonlinear response to visual flow. Equation (2) describes the relationship between motor output and DRN activity: DRN activity suppresses motor output, but the effect increases more slowly the stronger the DRN is activated and asymptotes to 1. We did not model the dynamics of the downstream effects of serotonin beyond this simple equation. Equation (3) describes visual feedback as a function of motor output, as it is also simulated in the experimental system.

QUANTIFICATION AND STATISTICAL ANALYSIS

Processing and Analysis of Fictive Swim Signals

Analyses of recorded swim signals were performed using custom-written scripts in MATLAB (Mathworks). The raw recorded signals were processed as described before (Ahrens et al., 2012; Vladimirov et al., 2014). In short, first slow fluctuations were removed from the raw signals by subtracting a smoothed version of the raw signal (using a Gaussian kernel with a 3.3 ms SD); this preserves the fast structure in the signal that represents the spikes in the motor nerve signal but removes slow signal drift. Next, the resulting signal was squared (to get the 'power' of the signal), and smoothed by applying the same Gaussian kernel (SD 3.3 ms, to get the 'local power' of the signal). The resulting traces are defined to be the swim signal, as shown in Figures 1, 2, 3, and 4. Individual swim bouts were detected by finding the time points at which the swim signal crossed a threshold, which was designed to lie just above the noise level of the swim signal. This threshold was found using a local histogram of the swim signal as described before (Ahrens et al., 2012; Vladimirov et al., 2014). The power of individual swim bouts was defined to be the area under the swim signal between the onset and offset of the detected swim bouts. The total locomotor drive in each task period was defined as the sum over the powers of all detected bouts within the task period. Swim bouts within the first 2 s of each task period were omitted from this calculation, except those in the test period in the short-term motor learning assay, where it was important to take into account the behavior at the start of the period. For the short-term motor learning experiment in Figure 1, to accurately correlate behavioral quantities with neuronal activity, the locomotor drive was further corrected for slow fluctuations in recording quality by normalizing, for individual trials, the locomotor drive in each period of the assay by the total locomotor drive in the entire trial.

In the short-term motor learning paradigm, the delay period served not only for testing the presence of the learning effect but also for the analysis of neural activity without the dynamic effect of behavioral and sensory input, which would generate neural responses not directly representing the learning effect. We therefore removed from the analyses trials in which the locomotor drive in the delay period was greater than 1/4 of the average locomotor drive in the last 5 s of the training period, and discarded fish that had more than 40% such trials. Similarly, to equalize as much as possible the behavior in the different training conditions – different durations of high-feedback-gain training – and to avoid that observed effects can be explained by slow behavioral variability over time, we required that the variability in locomotor drive in the last 5 s of the training period was less than 25% of the mean locomotor drive. Fish that displayed too much variability in their behavior over time tended not to satisfy this criterion and were not included in the analysis. Further, to avoid artifacts arising from tissue drift, fish that showed substantial tissue drift (> 1.5 μm, see below) during the experiment were removed from analyses in the calcium imaging experiments. The fractions of fish that passed these criteria were as follows: 12 out of 19 fish for the experiment in Figure S1A; 12 out of 39 fish for the experiment in Figure 1F and S1B; 6 out of 51 fish for the experiment in Figure S1D; 8 out of 117 fish for the experiment in Figure S1G; 11 out of 33 fish for the experiment in Figures 4F and S5C; 10 out of 31 fish for the pCPA experiment in Figure 6B, and 10 out of 33 fish for the non-treated control fish; 9 out of 22 fish for epNTR+ fish and 8 out of 30 fish for control epNTR- fish for the experiment in Figure 6D; 9 out of 19 fish for the

experiment in Figures 6E–6H; 7 out of 14 fish for the experiment in Figure S7G. All of the fish showed robust modulation of swim strength by changes in the motosensory gain. Fish that showed weak or no fictive swim signals during the fictive behavioral assays are not included in the above numbers.

In the behavioral paradigm illustrated in Figure S4A, only fish which swam less in in the stop period than in the closed-loop period were used for the analysis. 5 out of 10 fish passed the criterion and were used for the analyses.

The strength of the learning effect, which was used for subdividing the fish into two groups with either strong learning effect (Fish#1-6) or weak/no learning effect (Fish#7-12), was quantified as follows. A vector of locomotor drive in the test period [test^{7s}, test^{15s}, test^{30s}] was first normalized by the locomotor drive after 7 s of training [test^{7s}] and linear-fit using a time vector ([0 0.5 1]) representing the different training durations. The resulting gradient coefficient, which represents the total attenuation of test locomotor drive as a result of longer training, was used as an indicator of the strength of the learning effect and for sorting fish into the strong learning effect group (Figure 1F) and the weak/no learning effect group (Figure S3B).

The turning index used for the quantification of turning behavior in Figure S1E is defined as follows:

$$\textit{Turning index} = \frac{1}{N}\sum_{n=0}^{N-1}\left(\left(P_{L(n)}/\left(P_{L(n)}+P_{R(n)}\right)-0.5\right)\cdot S_n\right)$$

Here N represents number of events, S_n represents the index of stimulus flow direction (1 for leftward stimuli; −1 for rightward stimuli) in the probe, and $P_{L(n)}$ and $P_{R(n)}$ represent the normalized power of the signal at the left and right tail electrode channels at the nth swim event. Within each channel, normalization is performed by dividing by the average power of the channel at all the swim events in the initialization and training periods. To calculate laterality in the above expression, $P_{L(n)}$ is divided by the sum of $P_{L(n)}$ and $P_{R(n)}$ to confine the value between 0 and 1, and then 0.5 is subtracted so that opposite directions of fictive turning produce opposite signs.

Statistical Analysis

For comparisons of locomotor drive across multiple fish (Figures 1F, 4G, 6B, 6D, 6G, 6H, S1, S5C, S7D, and S7H), the locomotor drive or the power of first bout in the test period was averaged across trials and was further normalized, per fish, to the average across all conditions. This was done to compensate for variability across fish in the strength of fictive swimming. The locomotor drives, normalized and averaged within fish, were tested for statistical significance across fish by either a linear mixed effects model (LME) for the effect of training or delay durations (Figures S1A, S1B, and S5C), one-way ANOVA followed by Tukey's post hoc test (Figures 6G, 6H, and S7D), the Wilcoxon rank-sum test between 2 groups (Figures 6B and 6D), and the one-tailed Wilcoxon signed-rank test (Figures S1E, S1H, and S7H) unless otherwise stated in the figure legend. The reaction time in Figures 1E, 1F, S1C, S1F, and S1I was defined as time taken to initiate the first bout after the start of the test period. The reaction probability in Figures S1C, S1F, and S1I was defined as the probability of evoking swim behavior within the test period across trials. Error bars in figures represent SEM unless otherwise stated. All the statistical analyses were performed using custom-written scripts in MATLAB.

Processing of Light-Sheet Imaging Data

The time series of each plane was registered for XY translations by custom-written C/CUDA software accelerated with a GPU computing board (Tesla K20, Nvidia).

We evaluated the amount of tissue drift and deformation by rigid cross correlation, and discarded experiments in which the average drift across the brain was large enough to interfere with data quality. Specifically, after the XY registration, the drift in the XY and Z directions was calculated as follows. First, for every Z-plane, a reference image sequence throughout the experiment was calculated by averaging volumes in 2 min chunks (~120 images). Second, grid-wise (12 μm intervals) measurement points were set inside the brain at every plane (50 to 200 points, depending on amount of tissue in the plane). Next, the XY drift was calculated for each measurement point by comparing the image patches (40 μm square) around the measurement point of the reference image sequence to the one from the first 2 min. Z drift was also calculated by comparing the image patches from the reference image sequences to interpolated versions of those from nearby Z-planes of the first 2 min. Since drift accumulates over time, the final drift distance was defined using a linear fitting of the drift distances throughout the reference image sequence independently for each patch. Finally, to construct a measure of tissue stability, the XY and Z drift distances were smoothed across neighboring measurement points, and then averaged within a fish. Fish showing a total drift of more than 1.5 μm in either the XY or Z dimension even after the registration were removed from analysis, considering the small size (~5 μm) of zebrafish neurons. Through this criterion, only the datasets with high tissue stability were included in the analysis.

Individual neurons expressing H2B-GCaMP6f appeared as spheres, because the calcium indicator is predominantly nucleus-localized, facilitating the segmentation of the brain into individual neurons. Neuronal cell bodies were isolated with an algorithm as described in Figure S2B. Briefly, GCaMP-positive areas of the volume were coarse-extracted by binary thresholding based on absolute pixel intensity and local image contrast. Then local intensity normalization was performed on each pixel by calculating a relative rank of pixel intensity (0-1 from darkest to brightest) within a surrounding image patch (a circular region with a radius of 3.2 μm). The normalized image was further smoothed by an averaging kernel (a circular patch with a radius of 1.2 μm) and a pixel with a maximum value within a surrounding image patch (a circular patch with a radius of 2.4 μm) was identified as a centroid of a neuron. This process of local smoothing and maxima detection was iterated twice because we found that this maximized the

number of neurons correctly recognized. The accuracy of this recognition method was verified using images of the optic tectum across 12 imaging datasets for the behavior in Figure S1B. Approximately 79% ± 7% of neurons identifiable by eye were automatically recognized, and approximately 89% ± 5% of recognized objects matched with eye-identifiable neurons. After detecting neurons, time series of pixel intensity were extracted from the central part of individual neurons (a circular ROI with 1.2 μm radius, or 29 pixels).

To calculate the neuronal activity time courses, approximated by the relative fluorescence of the calcium indicator relative to the baseline fluorescence, or $\Delta F/F_0$, the following procedure was performed on each neuron. First, the average background pixel readout of the camera in darkness was subtracted from the fluorescence time series. Second, a sequence of reference time points was set in the center of every trial; these points were used for subsequent fitting of a baseline function. To each reference time point we assigned a value, which is calculated by averaging the fluorescence values within the bottom 30th percentile within the trial. Third, we fit a reverse exponential to the sequence of reference points, assuming a simple model for the bleaching process of the fluorophore, and used this function as the baseline fluorescence F_0. Lastly, the entire trace was divided by the baseline function and 1 was subtracted to generate the $\Delta F/F$ (short for $\Delta F/F_0$) time series. To avoid double-counting of the neurons across neighboring planes, we searched for overlapping neuron pairs and removed one of each pair whose noise correlation coefficient, a pairwise correlation of $\Delta F/F$ traces minus the trial-averaged response, exceeded 0.7, because by eye this removed neurons that were double counted. For overlay analyses across multiple fish (Figures 1H, S3B, and S4B), the XYZ coordinates of identified neurons were further mapped to a 'standard' brain, which is a detailed 3-dimensional volumetric image of a 6 d.p.f. brain of *Tg(elavl3:H2B-GCaMP6f)*^{jf7} taken by a confocal microscope (LSM710, Zeiss) and contrast-adjusted by histogram equalization using the FIJI software package (NIH). Mapping of individual brains to the reference brain was performed using the 'Coregister' function of the SPM8 toolbox (UCL), and the resultant transformation matrix was used for calculating new XYZ coordinates for individual neurons. One fish (#8) in the weak/no learning effect group (Figure S3B) was not well-aligned to the reference brain and thus removed from overlay analysis in Figure S3B. Robustness of analysis results to the specifics of the baseline calculation was further confirmed by independently applying a different calculation method based on a moving percentile.

Analysis of Light-Sheet Data for Finding Neurons Encoding Behavior and Task Related Quantities

For all analyses, we focused on neurons whose responses were reliable across multiple task trials. For extracting such neurons, we created a matrix of the average $\Delta F/F$ in each task period (12 periods for the experiment in Figure 1E, consisting of 4 periods of [initialization, training, delay, test] for 3 different training durations; 3 periods for the experiment in Figure S4A) in every trial and performed one-way ANOVA across trials for individual neurons. In this way typically 25,000 to 40,000 neurons with significant p values ($p < 0.01$) for response reliability were extracted from individual fish and used for subsequent analyses.

For the extraction of neurons whose activity correlated with our measure of the strength of the learning effect (Figure 1H), neurons were further selected by the requirement that they are tuned to different gain levels. Two-sample t tests between average $\Delta F/F$ values in the low motosensory gain periods and those in the high motosensory gain periods across trials were performed for individual neurons, and neurons which were significant for both of the p values of the ANOVA (for response reliability) and the t test (for gain tuning) were used for further analysis. For extraction of learning-effect-encoding neurons we set two parameters (see Results). For the calculation of parameter (1), i.e., the training-duration-dependent activity change ('delay $\Delta F/F$ gradient' in Figure 1G), $\Delta F/F$ values were averaged over the last 3 s of the delay periods, and a vector of [$\Delta F/F_{7s}$, $\Delta F/F_{15s}$, $\Delta F/F_{30s}$] was linear-fit to a time vector [0 0.5 1] representing different training durations. The resulting gradient coefficient, which reflects the total $\Delta F/F$ change resulting from longer training, was further normalized by the dynamic range of $\Delta F/F$ of individual neurons. For the calculation of parameter (2), i.e., the behavioral correlation ('Prediction of test locomotor drive' in Figure 1G), the Spearman rank correlation coefficient between the mean $\Delta F/F$ values in the last 3 s in the delay period and the locomotor drive in the test period of the matching trials were calculated for individual neurons. For the overlay analysis across multiple fish in Figure 1H, the threshold for parameter (1) 'delay $\Delta F/F$ gradient' was set to either 0.05 or −0.05, and the threshold for parameter (2) 'Prediction of test locomotor drive' was set to either −0.15 or 0.15. To further extract neurons which were conserved across multiple fish, the following additional spatial filter was applied: an extracted neuron which passed the thresholding operation was mapped only if more than 3 neurons of the same type exist within a 30 μm spherical volume around the neuron in the reference brain in all the fish used for the overlay. The images of extracted neurons were convolved with a 3-dimensional Gaussian filter (SD 6 μm) to compensate for the variability in brain morphology and registration to the reference brain and overlaid across 6 fish exhibiting a strong learning effect (Figure 1H) or 5 fish exhibiting weak/no learning effect (Figure S3B). Per fish, 206 ± 26 (cyan) and 220 ± 33 (magenta) (mean ± SEM) neurons were extracted for fish exhibiting a strong learning effect, and 53 ± 6 (cyan) and 68 ± 11 (magenta) neurons were extracted for fish exhibiting weak/no learning effect using the above criteria. One fish in the weak/no learning effect group could not be aligned to the reference brain with the method used and was thus excluded from the analysis (see above).

For making the functional map of Figure S4B, neurons were extracted by ANOVA analysis as described above and were classified according to the period in which their activities were at the highest. To extract neurons that are conserved across multiple fish, the same spatial filter as described above for Figure 1H was applied to the 5 fish. Brain regions were identified according to available anatomical maps of the larval zebrafish brain (Randlett et al., 2015; Ronneberger et al., 2012).

Analysis of High-Speed Imaging Data

For the analysis of high-speed imaging of DRN neurons in Figures 2, 3, S4D, and S4E, we first performed the same behavioral paradigm as in Figure S4A that contains a period of open-loop forward grating presentation and a closed-loop period. To select for neurons that were preferentially active in closed-loop, DRN neurons that showed reliable activation across trials, and showed highest activity during the closed-loop period, were extracted by ANOVA analysis as described above (section 'Analysis of light-sheet data for finding neurons encoding behavior and task related quantities'). In all the analyses of fast imaging data for investigating the sensory and motor response properties of DRN neurons, locomotor drive and visual velocity traces were binned to the imaging frequency (30Hz). Based on the activity patterns related to individual swim events in closed-loop, we classified DRN neurons into two types: group 1 neurons (Figure 2A and 2B) which show transient responses right after swim events; and group 2 neurons (Figure S4D) which were suppressed right after swim events and then increased their activity levels until the next swim bout occurred. Group 1 and group 2 neurons were classified based on the gradient of their swim-triggered-average activity trace in a period of 200 ms just before swim onset in the stochastic gain paradigm (Figures 2 and 5) or in the closed-loop period of the paradigm used in Figure 3. A linear curve was fit to the ΔF/F values in a 200 ms window (6 measurement points) before swim onset; if the gradient of this curve was above 0.003 ΔF/F per 200 ms, i.e., average activity ramped up just before swim bouts, the neuron was classified as belonging to group 2; otherwise it was classified as a group 1 neuron. We quantified the fast responses of DRN group 1 neurons by their change in activity after individual swim and visual events. To do this we defined a baseline and a peak time point, and neuronal responses related to each swim event were quantified by subtracting the baseline ΔF/F from the next peak ΔF/F (Figure 2B). The baseline time point was set individually for each neuron to the point in a window of 500 ms before the swim bout when the average activity level of the neuron was lowest, and the baseline ΔF/F was defined to be the average ΔF/F within a 100 ms window around that time point. For individual group 1 neurons, the peak time point was set to the time of maximum average ΔF/F in a window of 1.3 s after swim bout onset, and the peak ΔF/F value was defined to be the average ΔF/F in a 100 ms period centered on that point (Figure 2B).

For the analysis in Figure 2, we included only neurons that showed a response to the swim and stimulus events. Specifically, neurons which showed average ΔF/F responses per swim event (maximum in a 1.3 s window as described above) over a threshold value (0.01) in either low, medium, or high motosensory gain conditions (57% ± 6% of analyzed neurons across 21 fish) were included in the analysis.

For the analysis in Figure 3, group 1 neurons that showed average ΔF/F responses per swim event over a threshold value (0.01) in the closed-loop period under high motosensory gain (Figure S4F) were included in the analysis. The numbers of group 1 neurons per fish used for the analysis were as follows (mean ± SEM across fish): 10 ± 1.3 from the DRN for the analysis of Figures 2E and 2F; 7.0 ± 1.9 from the DRN and 5.5 ± 0.5 from the optic tectum for the analysis of Figure 3D. Fish with fewer than 2 neurons exceeding the threshold were excluded from analyses (2 out of 23 fish). Average responses across neurons were calculated within a fish, and further averaged across the fish. Swim bouts closer than 600 ms from either the preceding or following swim bout were discarded from the analysis to avoid cross-talk between swim events. To avoid including abnormal behavioral events, swim bouts with more than 5 s to the next swim bout were excluded from the analysis. Events with visual motion events lasting more than 400 ms were also discarded to avoid spillover artifacts in the analysis, where long visual input might bleed into the next swim bout even though the onset times are temporally offset. Time bins of 233 ms (7 frames at 30 Hz imaging) were used to analyze the effect of onset time differences between motor output and visual motion on neuronal responses. The visual response values in Figure 3D are defined to be the ΔF/F values at a neuron-specific time lag after visual motion onset; this time lag was derived from the response profiles in the closed-loop period. It was defined for each cell to be the time between visual motion onset (and motor onset since it was in closed-loop) and the peak of the average triggered ΔF/F trace within 1.3 s after motion onset (800 ± 57 ms across 15 fish).

Analysis of Cell-Type Specific Imaging Data from *tph2*+ or *gad1b*+ Neurons in the DRN

For the analysis of Figures 5A–5F, DRN neurons which showed reliable activation across trials of the short-term motor learning paradigm were extracted by ANOVA analysis as described above (section 'Analysis of light-sheet data for finding neurons encoding behavior and task related quantities'). Pixel intensities of RFP fluorescence in individual neurons were quantified, and neurons whose RFP intensities were higher than the population SD plus the population average were regarded as positive for RFP expression. The number of neurons per fish used in the analysis was as follows (mean ± SEM across fish): 60 ± 7.5 from 7 fish for *tph2*+ DRN neurons, and 40 ± 3.7 from 9 fish for *gad1b*+ DRN neurons.

For the analysis of fast activity kinetics of *tph2*+ or *gad1b*+ neurons in Figures 5G–5J, S5E, and S5F, RFP+ neurons were manually selected based on the RFP image, and activity traces of individual neurons were extracted. For the analysis of Figure 5G–5J, neurons which showed reliable activity patterns across trials in the short-term motor learning paradigm were first extracted by ANOVA analysis as described above (section 'Analysis of light-sheet data for finding neurons encoding behavior and task related quantities'), and were further classified into subgroups depending on their activity patterns during the short-term motor learning paradigm (Figures 5B and 5E). The numbers of neurons per fish used for the analysis were as follows (mean ± SEM across fish): 6.9 ± 1.0 per fish from 11 fish for *tph2*+ group 1 neurons (Figure 5G), 4.1 ± 1.1 from 8 fish for *gad1b*+ 'motor' type neurons (Figure 5I).

To quantify how the fast responses after individual swim events encoded the visual stimulus and the behavior, we fit linear models using the following procedure within individual fish to the datasets from the stochastic gain paradigm: for individual swim events, we quantified (1) power of the swim bout, (2) the maximum speed of visual feedback and (3) the average ΔF/F response across neurons. After normalizing each array of variables by their own mean and SD, (3) the average ΔF/F was linear-fit by (i) the power of swim bouts

and (ii) speed of visual feedback, and the resulting coefficients and residuals were calculated for individual fish. These coefficients were then tested for significant deviation from zero (Figures 5H and 5J). No significant residuals were observed in the fitting analyses.

Approximation of Single Spike Calcium Response from Imaging with Electrophysiology

For simultaneous recording of the nuclear-localized GCaMP6f signal and spiking activity (Figure S2C), a neuron in the optic tectum was imaged at 5 Hz by the custom two-photon microscope described above while recording spontaneous spikes by loose patch recording (with a MultiClamp 700B amplifier). The estimated GCaMP6f response kernel to a single spike in Figure S2D was calculated by assuming the following linear model, $\Delta F/F(t) = \sum_{\Delta t} CIRF(\Delta t) \cdot spike(t-\Delta t)$, where the calcium impulse response function (CIRF) is the model for the single-spike $\Delta F/F$ response, spike is a binary vector containing 0's for time points without spikes and 1's for time points with spikes, and the sum is over $\Delta t = -10$ s to +10 s in steps of 0.2 s (CIRF for $\Delta t < 0$ should be close to zero and these values were only included as a control). This linear model can be written in matrix form as $(\Delta F/F) = SPIKE \cdot CIRF$ with the matrix $SPIKE_{t,\Delta t} = spike(t-\Delta t)$, which can be inverted to recover CIRF (e.g., in MATLAB, after adding a column of 1's to SPIKE to allow for an additive offset and using the pseudoinverse, CIRF = SPIKE \ ($\Delta F/F$)).

DATA AND SOFTWARE AVAILABILITY

The software for image registration, calculation of brain deformation and neuron detection described in QUANTIFICATION AND STATISTICAL ANALYSIS can be found at https://github.com/ahrens-lab/Kawashima_et_al_Cell_2016/

Additional resources can be found at https://www.janelia.org/lab/ahrens-lab/resources-kawashima-etal-2016

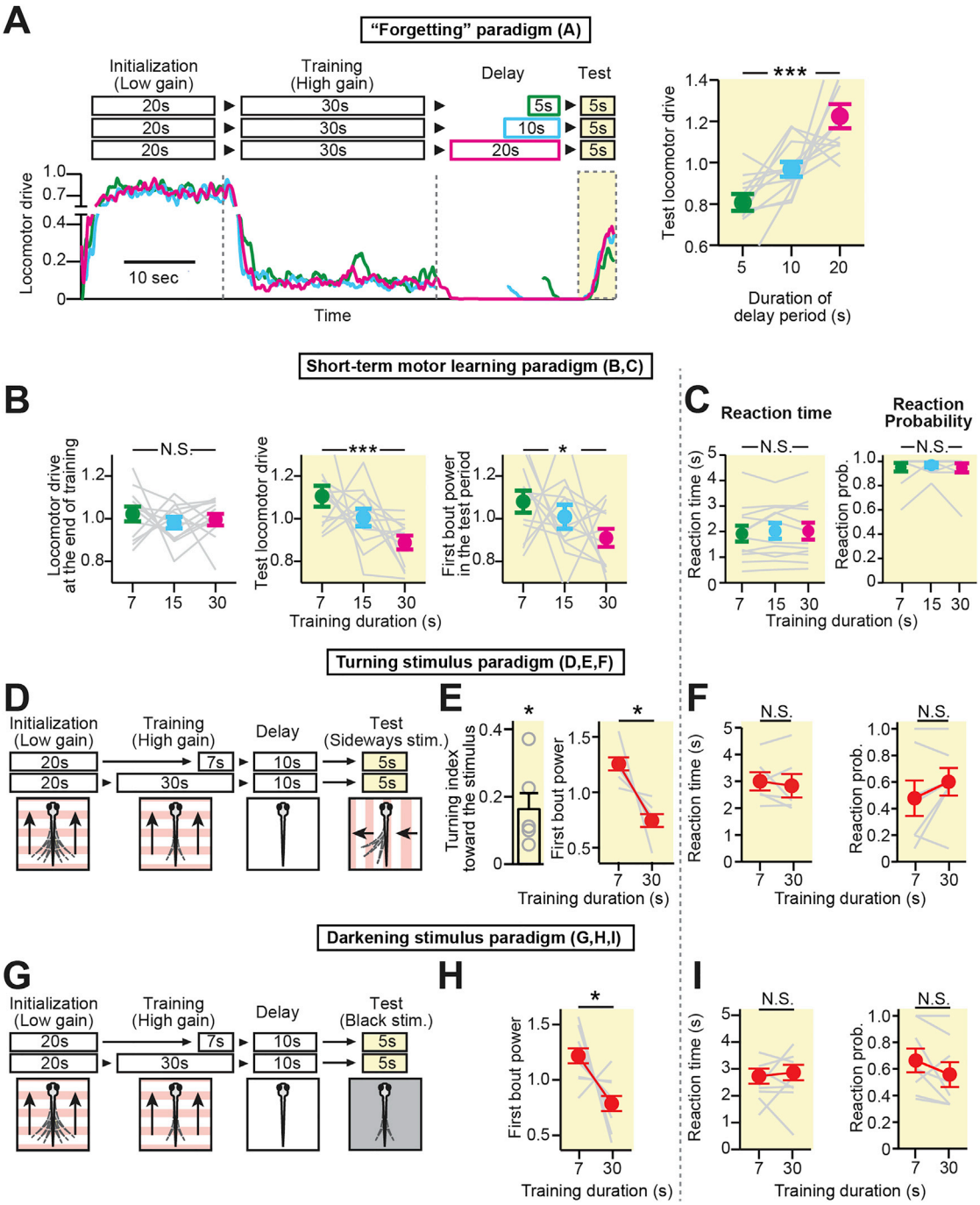

Figure S1. Statistics, Decay Dynamics, and Generalization of Locomotor Learning Effects, Related to Figure 1

(A) Time course of the learning effect in a 'forgetting paradigm' related to the short-term motor learning paradigm in Figure 1. *Left*, 'forgetting' paradigm for testing the persistence of the established learning effect, and an average swim trace from a representative fish. The duration of the delay period was set to 5 s (blue), 10 s (green), or 20 s (magenta). *Right*, comparison of locomotor drive in the test period. ***$p = 8.7 \times 10^{-5}$ for the effect of delay duration by linear mixed model (LME) across 12 fish. Gray lines represent data from individual fish. Error bars: SEM across fish.

(B) Quantification and statistics of behavior in the short-term motor learning paradigm described in Figures 1D–1F in all 12 fish. *Left,* locomotor drive at the end (5 s) of the preceding training period is unaffected by the training duration; N.S., p = 0.51 for the effect of training duration by LME. *Center,* in the test period, the locomotor drive is attenuated more heavily when training duration is longer. ***p = 0.00047 for the effect of training duration by LME across 12 fish. *Right,* in the test period, the power of the first swim bout is attenuated when training duration is longer. *p = 0.015 for the effect of training duration by LME across 12 fish. Error bars: SEM across fish.

(C) Quantification of reactivity in the test period of the short-term motor learning paradigm in Figures 1D–1F in all 12 fish. *Left*, reaction time to the test stimulus was unaffected by the training duration. N.S., p = 0.32 for the effect of training duration by LME across 12 fish. *Right*, reaction probability in the test period was

(legend continued on next page)

unaffected by the training duration. N.S., p = 0.11 for the effect of training duration by LME across 12 fish. Gray lines represent data from individual fish. Error bars represent SEM across fish. See STAR Methods for details of the normalization procedure and statistics.

(D) Learning effect on turning behavior. *Left*, the behavioral paradigm. In the initialization period, fish were exposed to low motosensory gain for 20 s, and in the training period to high motosensory gain for either a short (7 s) or long (30 s) period of time as in Figure 1E. After a 10 s delay period, a sideways-moving grating was presented to elicit turning behavior in the test period, and the power of first swim bout was quantified.

(E) Quantification of the behavior in (D). *Left*, as expected, fish perform fictive turns in the direction of visual motion, as reflected by the tuning index (see the STAR Methods for details). *p = 0.019 for one-sample t test. *Right,* the normalized power of the first bout in the test period is significantly attenuated after longer training (30 s). *p = 0.016 by one-tailed Wilcoxon signed-rank test across 6 fish for the effect of suppression after longer training. Error bars: SEM across fish.

(F) Quantification of reactiveness during the test period in (D). *Left*, reaction time in the test period was unaffected by training. N.S, p = 0.69 by Wilcoxon signed rank test across 6 fish. *Right*, reaction probability in the test period was unaffected by training. N.S, p = 0.25 by Wilcoxon signed rank test across 6 fish. Gray lines represent data from individual fish. Error bars: SEM across fish.

(G) Learning effect on the reaction to a darkening stimulus. *Left*, the behavioral paradigm. Fish were initialized under low motosensory gain for 20 s, and trained under high motosensory gain for either a short (7 s) or long (30 s) period of time in the same way as in Figure 1E. After a 10 s delay period, a dark scene was presented underneath the fish to elicit a swim reaction, and the power of the first swim bout was quantified. The stimulus was dark but not completely black.

(H) Quantification of the behavior in (G). The normalized power of the first bout in the test period in response to the darkening stimulus is significantly attenuated after longer training (30 s). *p = 0.027 by one-tailed Wilcoxon signed rank test across 8 fish for the effect of suppression after longer training. Error bars: SEM across fish.

(I) Quantification of reactivity during the test period in (G). *Left*, the reaction time in the test period was unaffected by training. N.S, p = 0.69 by Wilcoxon signed rank test across 8 fish. *Right*, reaction probability in the test period was unaffected by training. N.S, p = 0.25 by Wilcoxon signed rank test across 8 fish. Gray lines represent data from individual fish. Error bars: SEM across fish.

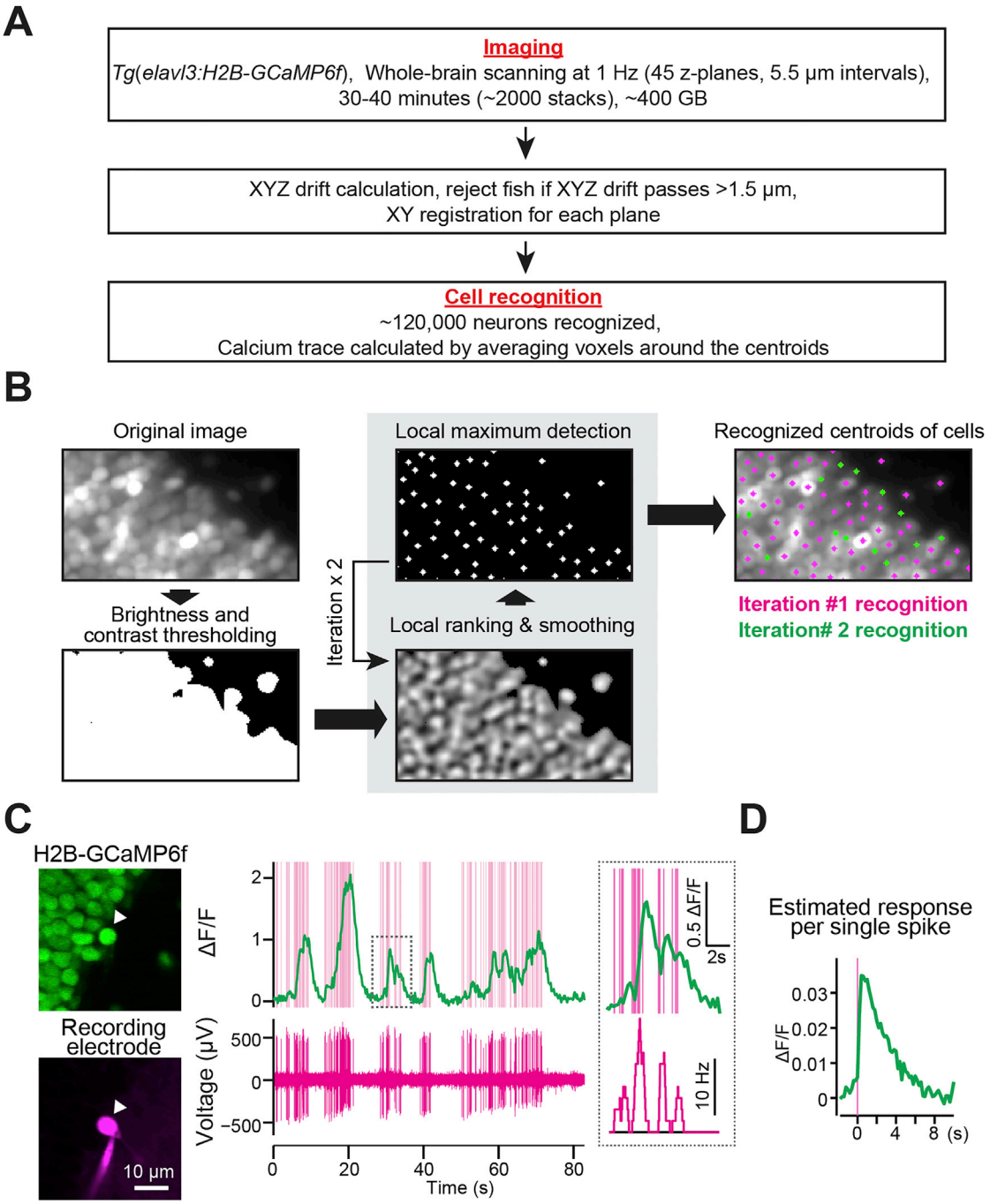

Figure S2. Data Processing and Cell Segmentation Pipeline for Whole-Brain Imaging Data, Related to Figure 1 and STAR Methods

(A) Schematic of the data processing pipeline. Details are provided in the STAR Methods.

(B) Overview of the cell recognition algorithm. After thresholding by brightness and local contrast, images are locally normalized and smoothed. Local maxima in the resulting image are assumed to be centroids of cell bodies. This process is iterated twice to assure maximum cell recognition. Details of the algorithm are provided in the STAR Methods.

(C) Simultaneous recording of the fluorescence signal of H2B-GCaMP6f and spiking activity from a single neuron by cell-attached recording. *Left*, the image of a recorded neuron (top) in the optic tectum and recording pipette filled with a red dye (bottom). The recorded neuron (arrowhead) is electroporated with the red dye after the recording. *Center*, time course of normalized fluorescence (top, green) and spontaneous spiking activity (bottom, magenta) of the same neuron. Detected spikes are drawn behind the normalized fluorescence (magenta) for direct comparison. The fluorescence time course within the dashed lines is expanded on the right. *Right*, expanded time course of normalized fluorescence (top, green) and instantaneous spike rate in a sliding window of 500 ms (bottom, magenta).

(D) Estimated single-spike response (green) of fluorescence of H2B-GCaMP6f based on the data in (C). Magenta line represents spike onset.

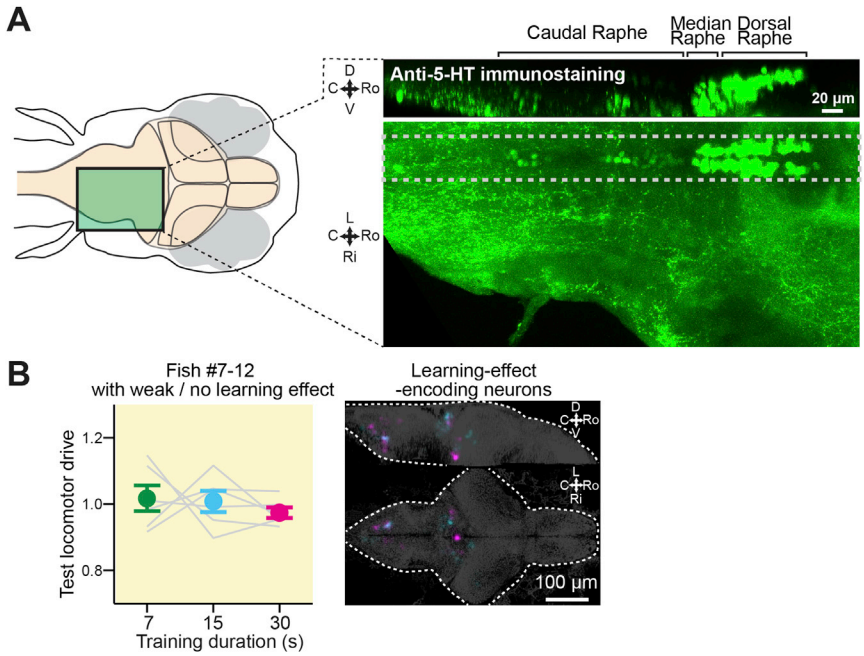

Figure S3. Anatomy of Serotonergic Neurons in the DRN, Related to Figure 1

(A) Distribution of 5-HT positive neurons in the hindbrain. *Left,* schematic diagram of hindbrain region imaged with a confocal microscope. *Right*, maximum intensity projection of 5-HT immunostaining from the side (top) and the top (bottom) of the hindbrain. The side view is a maximum intensity projection of the tissue between the dashed gray lines in the top projection. Serotonergic clusters were classified and labeled above the top panel according to previous literature (Lillesaar et al., 2009; Parker et al., 2013). D, dorsal; V, ventral; Ro, rostral; C, caudal; Ri, right; L, left.

(B) *Left,* effect of training duration on behavior in the test period, as described in Figures 1D–1F, in the fish group with weak/no learning effect. Error bars: SEM across fish. Gray lines represent data from individual fish. *Right,* the overlaid map of learning-effect-encoding neurons in a fish group with weak/no learning effect at the behavioral level, showing far fewer neurons (53 ± 6 and 68 ± 11 neurons per fish for cyan and magenta neurons, respectively) that reach criterion compared to fish with strong learning effect in Figure 1H (206 ± 26 and 220 ± 33 neurons per fish for cyan and magenta neurons, respectively). Neurons are extracted by the same parameters (1) and (2) as explained in the main text and Figures 1G and 1H. D, dorsal; V, ventral; Ro, rostral; C, caudal; Ri, right; L, left.

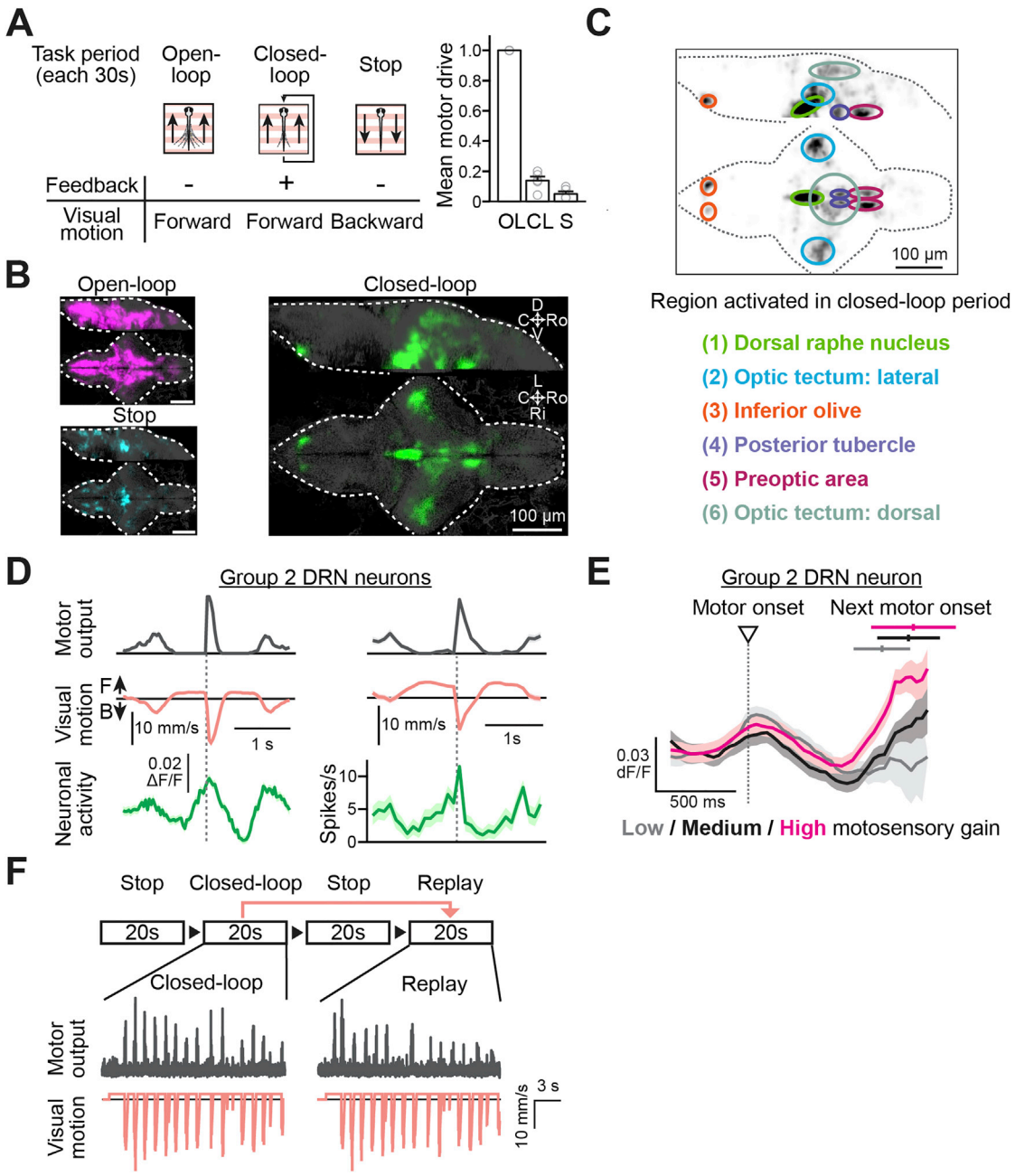

Figure S4. Whole-Brain Map of Neurons that Are Responsive to Closed-Loop Visual Feedback, and Activity Patterns of Group 2 DRN Neurons, Related to Figures 2 and 3

(A) The behavioral task for identifying neurons activated by closed-loop sensory feedback. *Left*, illustration of the behavioral task. In the 'open-loop' period, the visual environment moves forward without any feedback. In the 'closed-loop' period, the visual environment moves forward, but when a swim signal is detected it moves backward. In the 'stop' period, the visual environment slowly moves backward, during which the fish tend to swim less or cease swimming. *Right*, normalized locomotor drive in the open-loop (OL), the closed-loop (CL) and the stop (S) period. Locomotor drives of individual fish are normalized to their average locomotor drive in the open-loop period. Error bars represent SEM across 5 fish.

(B) Whole-brain maps of neurons that showed highest activity in the open-loop period (magenta, left top), in the closed-loop period (green, right) and in the stop period (cyan, left bottom) morphed and overlaid on a reference brain (gray). n = 5 fish. See the STAR Methods for details of analyses. D, dorsal; V, ventral; Ro, rostral; C, caudal; Ri, right; L, left.

(C) Anatomical segmentation of brain regions that showed highest activity in the closed-loop period. *Top*, the same whole-brain map in (B) inverted for brightness and overlaid with anatomical masks. *Bottom*, a list of 6 identified anatomical regions.

(D) Top, a representative average ΔF/F activity trace (green, bottom left) and a representative electrophysiologically recorded spiking pattern (green, bottom right) from two group 2 DRN neurons recorded separately. Average swim trace is shown in gray (top) and the average visual motion in the virtual reality environment is

(legend continued on next page)

shown in orange (middle). Gray dotted lines represent the onsets of swim bouts to which the averaged traces are aligned. Shadows represent SEM across averaged swim events.

(E) Average ΔF/F activity trace of a representative group 2 neuron in the DRN in response to different motosensory gains during the stochastic gain paradigm. The delayed response is stronger under high motosensory gain (magenta) than under medium (black) or low (dark gray) motosensory gain. The onset time (mean ± SD) of the next swim bout is indicated on the top. For each swim bout, only the activity trace up to the onset of the following bout is included in the average.

(F) Behavioral task for desynchronization of swim bouts and visual flow as described in Figure 3B. In the 'stop' period of 20 s, the visual motion is stopped. In the 'closed-loop' period of 20 s, the visual environment moves forward, but when a swim signal is detected, it moves backward with high motosensory gain. In the 'replay' period of 20 s, the same visual motion (orange, bottom) as in the preceding closed-loop period is replayed and the swim events (gray, middle) are desynchronized with visual motion as also shown in Figure 3B.

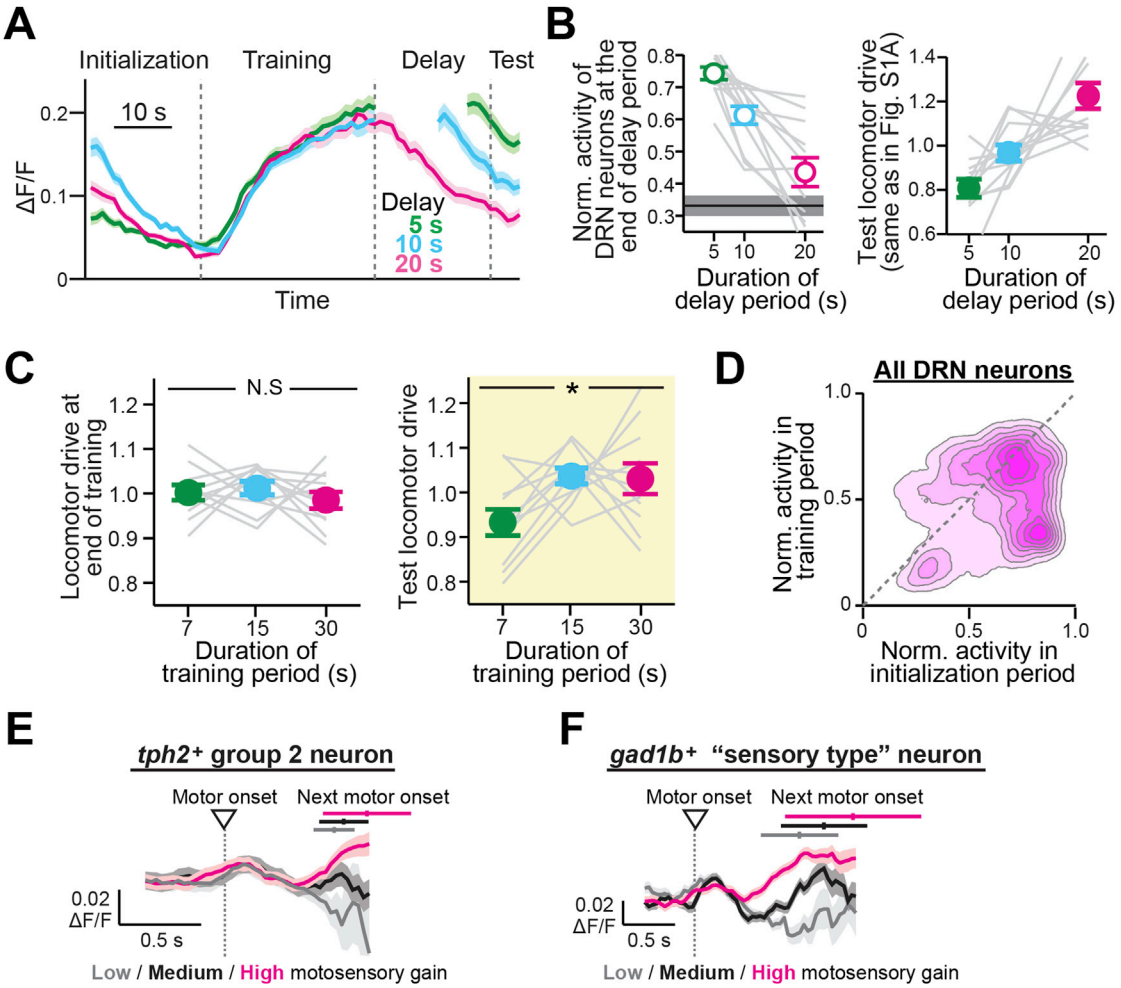

Figure S5. Activity of DRN Neurons during an Extended Set of Short-Term Motor Learning Paradigms, Related to Figures 4 and 5

(A) Average calcium traces of 89 DRN neurons from a representative fish performing the forgetting task presented in Figure S1A. Activity traces of neurons that show highest activity during the delay period were extracted and averaged. Shadows represent SEM across averaged neurons.

(B) *Left*, quantification of activity decay kinetics of DRN neurons across the same 12 fish used in Figure S1A. DRN neurons that show higher activity during the training period than in the initialization period were extracted and their average activity traces across trials were normalized by the minimum and maximum values of the average traces. Normalized activity levels in the last 3 s of the delay period were quantified in each neuron, averaged across neurons, and further averaged across 12 fish. Error bars represent SEM across fish. The black line and gray shadow at the bottom represent the mean and SEM of activity levels in the initialization period. *Right*, locomotor drive in the test period after different delay durations. The same data as in Figure S1A are re-plotted for comparison. Error bars represent SEM across fish. Gray lines represent data from individual fish.

(C) *Left*, comparison of locomotor drive at the end of the training period in the motor learning paradigm described in Figure 4F in all 11 fish. N.S., $p = 0.47$ for the effect of training duration by LME across 11 fish. *Right*, comparison of locomotor drive in the probe period. *$p = 0.018$ for the effect of training duration by LME across 11 fish. Error bars represent SEM across 11 fish. Gray lines represent data from individual fish.

(D) Comparison of neural activity levels in the initialization and training periods of all DRN neurons across 11 fish from the motor learning paradigm in (D). 3,294 DRN neurons from 11 fish are plotted and smoothed as in Figure 4A.

(E) Average ΔF/F activity trace of a representative *tph2*+ group 2 serotonergic neuron in the DRN in response to swim events under different motosensory gains in the stochastic gain paradigm. The response is stronger under high motosensory gain (magenta) than under medium (black) or low (dark gray) motosensory gain. The onset time (mean ± SD) of the next swim bout is indicated on the top. For swim each bout, only the activity trace up to the onset of the following bout is included in the average.

(F) Average ΔF/F activity trace of a representative *gad1b*+ neuron in the DRN, selected for having higher activity during the training period (Figure 5E), in response to different motosensory gains in the stochastic gain paradigm. The response is stronger under high motosensory gain (magenta) than under medium (black) or low (dark gray) motosensory gain. The onset time (mean ± SD) of the next swim bout is indicated on the top.

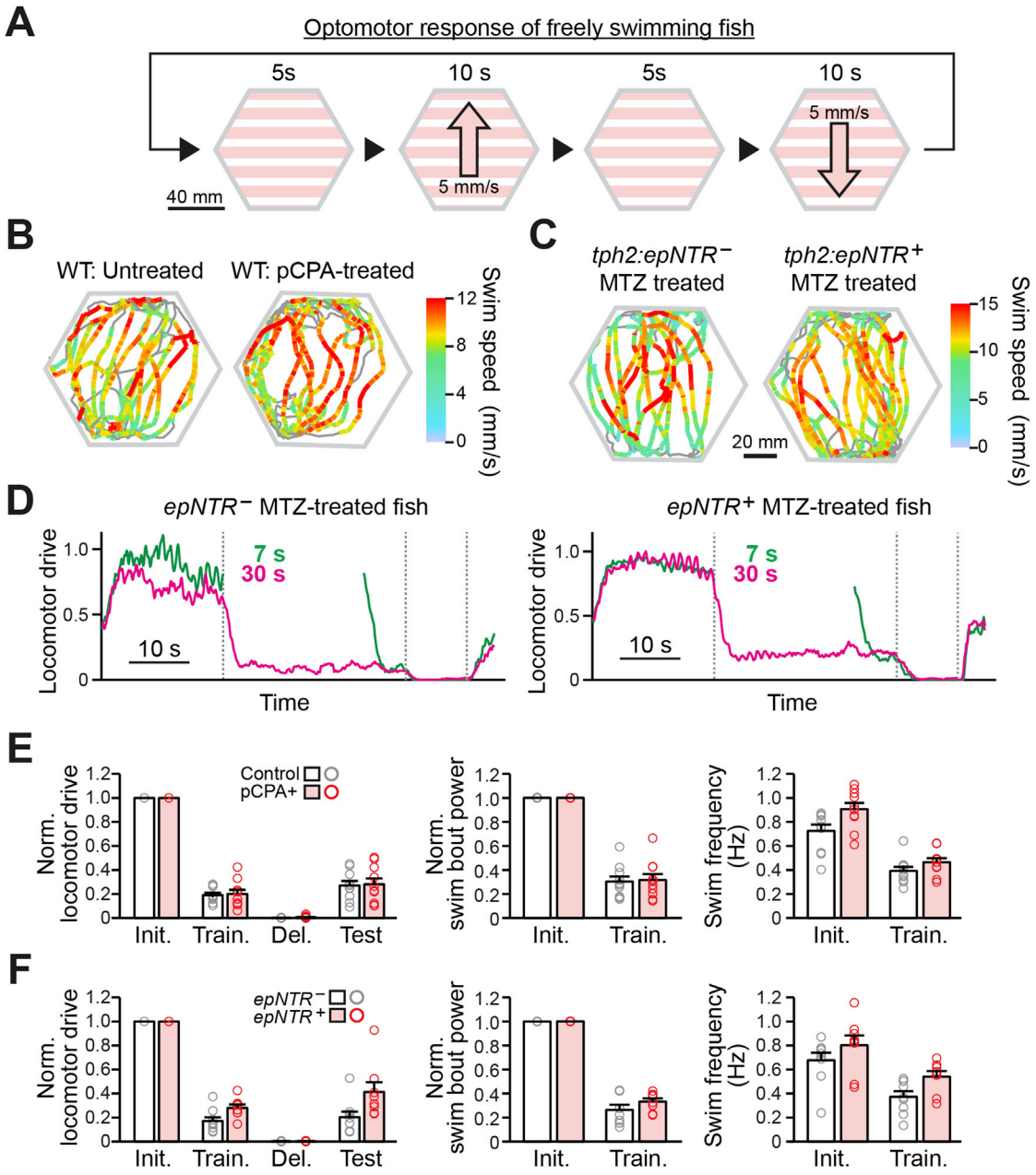

Figure S6. Behavioral Characterization of pCPA-Treated Fish and Genetic Chemically Ablated Fish, Related to Figure 6

(A) Behavioral paradigm for evaluating the optomotor response (OMR) in freely swimming fish. The fish was placed in a hexagonal plastic dish filled with water, and moving gratings were projected onto the bottom of the dish. Stationary gratings were presented for 5 s, after which the grating was moved at a speed of 5 mm/s for 10 s to elicit the optomotor response. The direction of grating movement was flipped at every presentation to maximize the swim distance of fish across multiple trials.

(B) Swim trace of a representative control wild-type (WT) fish (*left*) and a pCPA-treated fish (*right*) during the freely swimming behavioral paradigm in (A). Gray lines represent swimming during the period of no grating movement, and colored lines represent temporally smoothed traces with swim speed color coded during the period of grating movements.

(C) Swim trace of a representative control *tph2:epNTR*(−) fish (*left*) and a *tph2:epNTR*(+) fish (*right*) during the free swimming behavior in (A) after treatment with metronidazole (MTZ).

(D) Behavior of a representative *tph2:epNTR*(-) fish (*left*) and a representative *tph2:epNTR*(+) fish (*right*) in the short-term motor learning paradigm. The fish are trained under high motosensory gain for short (7 s, green) or long (30 s, magenta) periods of time and the learning effect is measured in the test period.

(E and F) Quantification of population behavioral parameters of pCPA-treated fish used in Figures 6A and 6B (E) or of chemically ablated fish used in Figures 6C and 6D (F). Overall locomotor drive in the four task periods (*left*), power of individual swim bouts in the initialization and training periods (*center*) and frequency of

(legend continued on next page)

swim bouts in the initialization and training periods (*right*) were quantified for all the fish used in Figures 6A–6D; 10 fish for the control group and 10 fish for the pCPA-treated group in (E); 8 fish for *tph2:epNTR*(-) group and 9 fish for *tph2:epNTR*(+) group in (F). Overall locomotor drive in individual task periods (left) and power per swim bout (center) are normalized to the value in the initialization period for each fish to compensate for the variation of recording quality. Error bars represent SEM across fish.

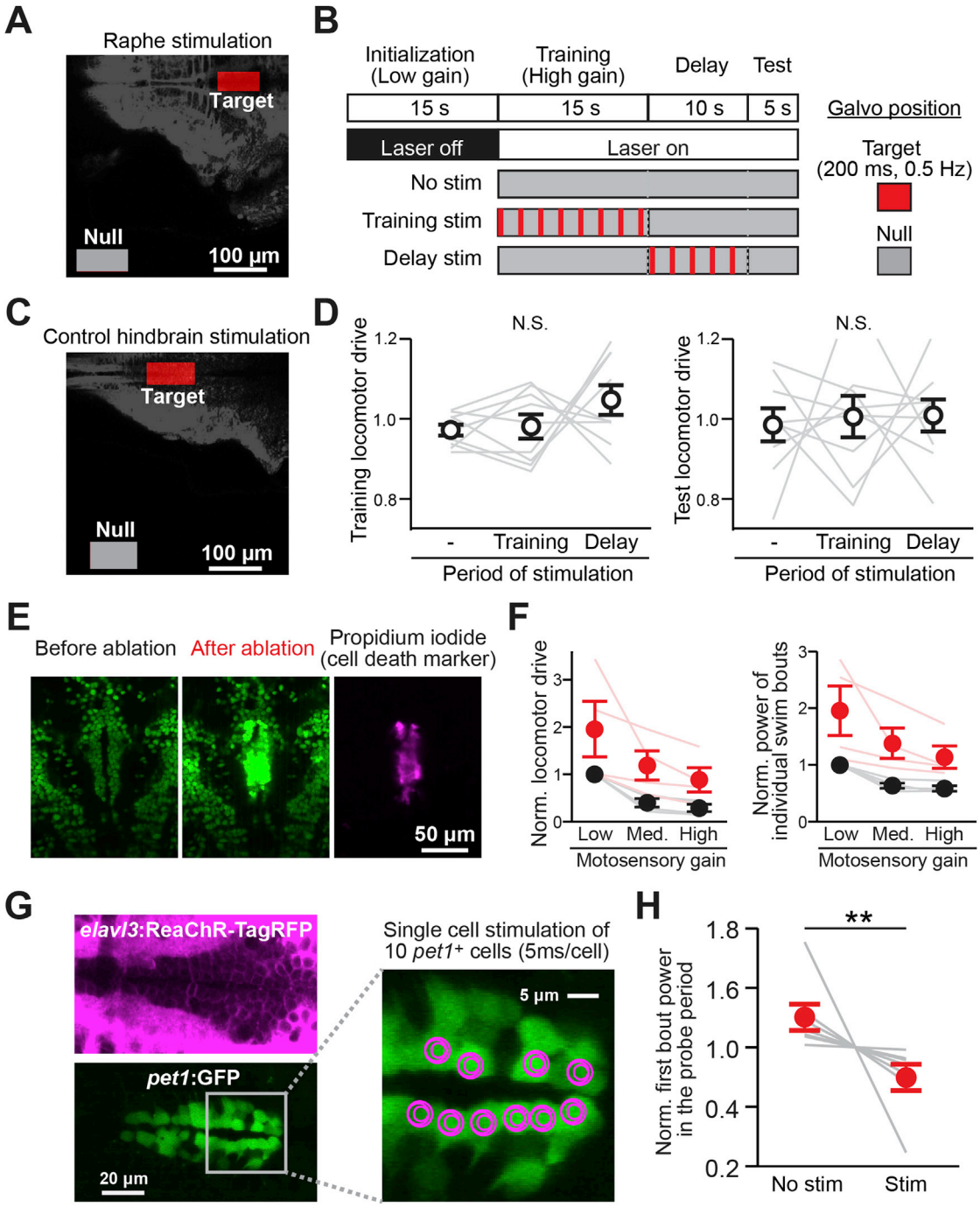

Figure S7. Optogenetic Activation and Laser Ablation of DRN Neurons, Related to Figure 6

(A) ROI settings for DRN stimulation. To stimulate DRN neurons, the target region is scanned, and to remove DRN stimulation, the null region is scanned (as an alternative to using a laser shutter, to avoid auditory stimulation by the rapid opening and closing of the shutter).

(B) Detailed stimulation protocol of the experiment presented in Figures 6E–6H. The default laser scan area was set to the 'Null' ROI outside the fish. During the period of stimulation, the laser scan area was moved to the 'Target' ROI for a short period of time (200 ms, performing four area scans of 50 ms each) once every 2 s.

(C) ROI settings for control hindbrain stimulation.

(D) Effect of control hindbrain stimulation on the locomotor drive in the training period (left) and the test period (right), showing no significant effects. N.S., $p = 0.15$ (left) and $p = 0.92$ (right) by one-way ANOVA across 9 fish. Error bars represent SEM across the same set of 9 fish as in Figures 6G and 6H. Gray lines represent data from individual fish.

(E) Two-photon plasma-mediated laser ablation of DRN neurons in *Tg(elavl3:H2B-GCaMP6f)*^{jf7} transgenic zebrafish. Dozens of cells in the DRN across multiple Z-planes were ablated; displayed here are images from a single plane. After ablation, the basal intensity of GCaMP fluorescence increased, indicating cell

(legend continued on next page)

damage. Cell death and its local confinement were further verified post hoc by staining with propidium iodide, a membrane-impermeable dye-specific to dead cells.

(F) Locomotor drive (left) and power of individual swim bouts (right) under various levels of motosensory gain before (black) and after (red) DRN cell ablation, showing an increase in locomotor drive following ablation. The fish are still able to perform real-time motor adaptation, which we also observed in the chemical genetic ablation results in Figures 6 and S6. Values were normalized to the average locomotor drive under low motosensory gain before ablation in individual fish. Error bars represent SEM across 4 tested fish. Two-way ANOVA was performed on the effect of ablation and motosensory gain. (Left) $p = 0.0045$ and (Right) $p = 0.0007$ between before and after ablation. No interaction in the two-way ANOVA test was detected between the effects of ablation and motosensory gain. Thin red lines and gray lines represent data from individual fish before and after ablation, respectively.

(G) Cell-type specific two-photon optogenetic activation of individual serotonergic neurons in the DRN. Double transgenic zebrafish which express ReaChR-TagRFP under the *elavl3* promoter (left top, magenta) and GFP in *pet1*+ serotonergic neurons (left bottom, green) [*Tg(elavl3:ReaChR-TagRFP-T; pet1:GFP)*] were used in this experiment. 10 *pet1*+ serotonergic neurons in the DRN were stimulated individually by local spiral scanning, with the scan pathway shown in magenta on the *right*. These neurons were stimulated 4 times in a 200 ms period (i.e., at 20 Hz within this window), with 5 ms spiral time per cell, timed to be 2 s before the end of the delay period (i.e., about 3 s before the first swim bout in the test period).

(H) Effect of stimulation during the delay period on the power of the first bout in the test period. The behavioral paradigm of this experiment is the same as the one in Figure 6F except that we only tested two conditions, control (No stim) and stimulation (Stim) as described in (G). $^{**}p = 0.0078$ from one-tailed Wilcoxon signed-rank test across 7 fish for the effect of suppression after stimulation. Gray lines represent data from individual fish. Error bars: SEM across fish.